AD-A174 005 EFFECT OF THERMOMECHANICAL PROCESSING ON THE ELEVATED TEMPERATURE BEHAVIO..(U) NAVAL POSTGRADUATE SCHOOL MONTEREY CA S B OSTER JUN 86 1/1

UNCLASSIFIED F/G 11/6 NL

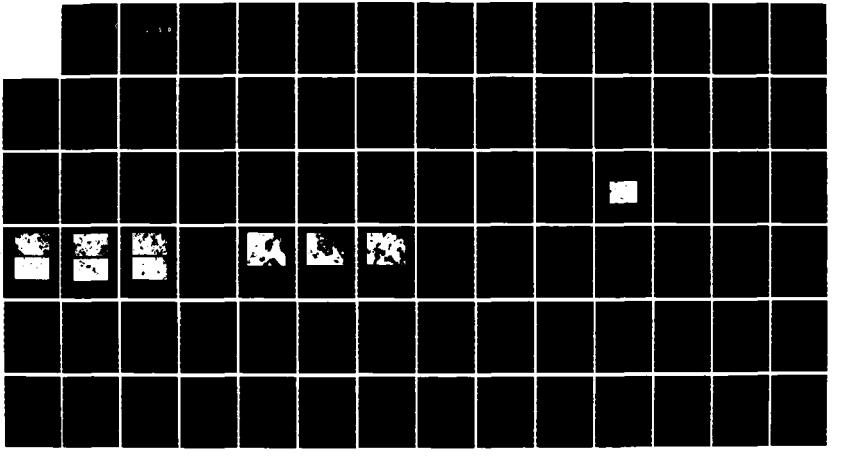

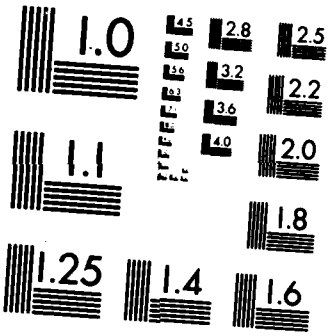

(2)

NAVAL POSTGRADUATE SCHOOL
Monterey, California

THESIS

EFFECT OF THERMOMECHANICAL PROCESSING ON THE ELEVATED TEMPERATURE BEHAVIOR OF LITHIUM-CONTAINING HIGH-Mg, Al-Mg ALLOYS

by

Stephen B. Oster

June 1986

Thesis Advisor: T. R. McNelley

Approved for public release; distribution is unlimited.

Unclassified
SECURITY CLASSIFICATION OF THIS PAGE

REPORT DOCUMENTATION PAGE

1a REPORT SECURITY CLASSIFICATION	1b. RESTRICTIVE MARKINGS
2a SECURITY CLASSIFICATION AUTHORITY	3 DISTRIBUTION / AVAILABILITY OF REPORT Approved for public release; distribution is unlimited.
2b. DECLASSIFICATION / DOWNGRADING SCHEDULE	
4 PERFORMING ORGANIZATION REPORT NUMBER(S)	5 MONITORING ORGANIZATION REPORT NUMBER(S)

6a. NAME OF PERFORMING ORGANIZATION Naval Postgraduate School	6b OFFICE SYMBOL (If applicable) Code 69	7a. NAME OF MONITORING ORGANIZATION Naval Postgraduate School	
6c. ADDRESS (City, State, and ZIP Code)		7b. ADDRESS (City, State, and ZIP Code)	
8a. NAME OF FUNDING / SPONSORING ORGANIZATION	8b. OFFICE SYMBOL (If applicable)	9. PROCUREMENT INSTRUMENT IDENTIFICATION NUMBER	
8c. ADDRESS (City, State, and ZIP Code)		10 SOURCE OF FUNDING NUMBERS	
		PROGRAM ELEMENT NO	PROJECT NO / TASK NO / WORK UNIT ACCESSION NO

11 TITLE (Include Security Classification)
EFFECT OF THERMOMECHANICAL PROCESSING ON THE ELEVATED TEMPERATURE BEHAVIOR OF LITHIUM-CONTAINING HIGH-Mg, Al-Mg ALLOYS

12 PERSONAL AUTHOR(S)
OSTER, Stephen B.

13a TYPE OF REPORT	13b TIME COVERED	14 DATE OF REPORT (Year, Month, Day)	15 PAGE COUNT
Master's Thesis	FROM _____ TO _____	1986 June	81

16 SUPPLEMENTARY NOTATION

17 COSATI CODES			18 SUBJECT TERMS (Continue on reverse if necessary and identify by block number)
FIELD	GROUP	SUB-GROUP	Al-Mg-Li, Superplasticity, Superplastic Deformation, Thermomechanical Processing

19 ABSTRACT (Continue on reverse if necessary and identify by block number)

An experimental investigation was conducted to determine the mechanical properties and microstructural characteristics resulting from thermomechanical processing by warm rolling of an Al-8.0%Mg-0.5%Li-0.15%Zr Alloy and an Al-8.0%Mg-1.0%Li-0.15%Zr Alloy. At ambient temperature, yield strengths were 38 to 44 Ksi (262-303 MPa), ultimate tensile strengths were 60 to 65 Ksi (414-450MPa), with 10-12% elongation to fracture. Both alloys were moderately superplastic at 300°C; an elongation of 340% was attained with the 1.0%Li alloy. Behavior of the alloy is consistent with continuous recrystallization during annealing and deformation at warm temperatures, and is very similar to that of previously studied Al-Mg-X alloys.

20 DISTRIBUTION / AVAILABILITY OF ABSTRACT	21 ABSTRACT SECURITY CLASSIFICATION	
☒ UNCLASSIFIED/UNLIMITED ☐ SAME AS RPT ☐ DTIC USERS	Unclassified	
22a NAME OF RESPONSIBLE INDIVIDUAL Terry McNelley	22b TELEPHONE (Include Area Code) (408) 646-2589	22c OFFICE SYMBOL 69Mc

DD FORM 1473, 84 MAR 83 APR edition may be used until exhausted
All other editions are obsolete

SECURITY CLASSIFICATION OF THIS PAGE
Unclassified

Approved for public release; distribution is unlimited.

Effect of Thermomechanical Processing on the Elevated Temperature Behavior of Lithium-Containing High-Mg, Al-Mg Alloys

by

Stephen B. Oster
Lieutenant Commander, United States Navy
B.U.S., University of New Mexico, 1975

Submitted in partial fulfillment of the requirements for the degree of

MASTER OF SCIENCE IN MECHANICAL ENGINEERING

from the

NAVAL POSTGRADUATE SCHOOL
June 1986

Author: _____

Approved by: _____
T.R. McNelley, Thesis Advisor

_____
Paul Marto, Chairman, Department of Mechanical Engineering

_____
John N. Dyer, Dean of Science and Engineering

ABSTRACT

An experimental investigation was conducted to determine the mechanical properties and microstructural characteristics resulting from thermomechanical processing by warm rolling of an Al-8.0%Mg-0.5%Li-0.15%Zr alloy and an Al-8.0%Mg-1.0%Li-0.15%Zr alloy. At ambient temperature, yield strengths were 38 to 44 Ksi (262-303 MPa), ultimate tensile strengths were 60 to 65 Ksi (414-450 MPa), with 10-12% elongation to fracture. Both alloys were moderately superplastic at 300°C; an elongation of 340% was attained with the 1.0%Li alloy. Behavior of the alloy is consistent with continuous recrystallization during annealing and deformation at warm temperatures, and is very similar to that of previously studied Al-Mg-X alloys.

TABLE OF CONTENTS

DEDICATION

"The secret things belong to the Lord...but the things revealed belong to us...." [Deuteronemy 29:29] This thesis is offered, in gratitude, to Him who opens doors to those who persist in knocking.

ACKNOWLEDGMENT

"As iron sharpens iron, so one man sharpens another." [Proverbs 27:17]

I would like to thank my advisor, Professor T. R. McNelley, for his expert guidance in the conduct of this study. I would further like to acknowledge the invaluable instruction and assistance given me by Dr. S. J. Hales in developing the necessary microscopy and photographic skills essential to sound metallurgical inquiry.

I. INTRODUCTION

The phenomenon of superplasticity was observed as early as 1920 [Ref. 1]. The initial observations aroused little more than academic curiosity since the systems in which it was first observed were of no technological value. Since 1964, however, its observation in an increasing number of alloy systems has produced a flurry of activity in commercial research laboratories. While the complete explanation for superplasticity has not been formulated, it may soon be possible to fabricate and process a variety of technologically useful alloys which will behave superplasticly when deformed at elevated temperatures. Superplastic Aluminum (Al), Titanium (Ti), and Nickel-based (Ni) superalloy materials have all been used successfully in commercial manufacture. The desireability of superplastic materials is related to considerations such as savings in the fabrication costs of complex shapes (where costly machining can be eliminated), and to aerospace applications where eliminating the need for fasteners translates by iterative processes to a manifold weight savings.

Superplasticity is broadly defined as the deformation process by which metals undergo large elongations without fracture. The general requirements for superplastic deformation (SPD) are commonly cited as an equiaxed grain structure with uniformly fine grain size, in a polyphase alloy with phases exhibiting similar ductilities at the temperature of deformation [Ref 2].

A disadvantage with many of the metals demonstrating superplastic behavior is their low ambient temperature strengths. For many applications a moderate-to-high strength alloy capable of SPD during forming would be highly desireable . Aluminum alloys, because of their widespread use in industry, have attracted a great deal of attention as promising candidates for development of superplastic properties. Work on high-Mg, Al-Mg alloys at the Naval Postgraduate School (NPS) has led to the development of Al-Mg-X compositions which exhibit superplastic response after suitable thermomechanical processing (TMP). This thesis is an extension of that earilier work at NPS, and investigates the warm temperature mechanical response of two Lithium-containing (Li), Al-Mg alloys.

II. BACKGROUND

A. PHYSICAL METALLURGY

1. Aluminum Alloy Systems

Aluminum alloys have found widespread use in industry principally due to their low density, good ductility, and high strength-to-weight ratios. This has made them particularly attractive in transportation related applications, notably aerospace and automotive designs. Aluminum alloys may be broadly divided into heat treatable, and non-heat treatable subgroups. The heat treatable alloys are strengthened by precipitation hardening, while the nonheat treatable alloys are strengthened by solid solution strengthening and strain hardening. Wrought products of Al-Mg alloys have been used successfully for many years in ambient temperature applications and exhibit good strength, forming, and welding characteristics.

2. Strengthening of Al Alloys

The effectiveness of all strengthening mechanisms depends ultimately on their ability to restrict the easy movement of dislocations

through the crystalline metallic lattice. Dislocations are line defects in the lattice, and are principally responsible for the slip process by which most metals deform plastically. Dislocations move with relative ease in pure metals, and consequently these metals show little strength. Thus, in order to obtain higher strengths, the mobility of these dislocations must be reduced.

a. Solid Solution Strenghtening

Creating a solid solution of solute atoms in a solvent crystal lattice invariably increases the strength of the alloy over that of the pure metal. The factors most affecting solid solution strengthening are [Ref. 3] :

1. Relative size factor
2. Relative modulus factor
3. Electrical interaction
4. Chemical interaction
5. Configurational interaction.

All rely for their efficacy on the degree to which they restrict dislocation mobility. In solid solution strengthening, where no hard precipitate is present to inhibit dislocation movement by pinning, clustering of solute atoms along dislocations results in a sort of "frictional" force that restricts dislocation mobility. Such a force is often refered to as

solute-drag. Most of the Al alloys derive some degree of strength from solid solution strengthening.

b. Dispersion Strengthening

Dispersion strengthening depends upon the introduction of an insoluble second phase to reduce dislocation mobility. Introduction of a second phase occurs when the solubility of the alloying element in the solvent metal is exceeded. Generally, the solubility of the second phase in a dispersion strengthened solvent matrix is low even at high temperatures [Ref. 3: p. 221]. The presence of a second phase precipitate which is relatively hard and brittle in comparison with the surrounding matrix impedes dislocation motion, resulting in higher strength. The insoluble second phase is most often refered to as a "dispersoid" to distinguish it from the second phase precipitate produced by age hardening (see below). The dispersoids are typically not coherent with the surrounding matrix. Coherency refers to the degree of crystallographic matching that exists between the second phase particle and the surrounding matrix. The crystalligraphic planes of a coherent precipitate have a definite relationship to, and are frequently continuous with, the crystalligraphic planes of the matrix. All other conditions being equal, the elastic strain

field surrounding an incoherent particle is not as effective in retarding dislocation motion through the lattice as is that of the coherent particle.

c. Precipitation Strengthening (Age Hardening)

Precipitation hardening, like dispersion strengthening, depends upon the introduction of a second phase to restrict dislocation motion. To be precipitation hardenable the second phase must exhibit decreasing solubility with decreasing temperature. Introduction of the second phase is achieved by first solution treating at a temperature sufficient to produce a single phase solid solution, and then quenching to a temperature below the solubility limit for the second phase. The temperature is then raised once again to allow formation of the second phase by diffusional processes. This requires temperatures typically on the order of $0.4T_m$, where T_m is the absolute melting temperature of the alloy. Growth of the second phase precipitate usually results in coherency with the matrix. Coherency produces widespread elastic distortion of the surrounding lattice, and dislocations can interact with the strain field surrounding the precipitate even if they only pass nearby.

3. Effect of Alloying Elements

a. Magnesium (Mg)

Magnesium, which has a density roughly 2/3 that of Aluminum and a lower modulus of elasticity, is often used as an alloying addition to Aluminum. It may be used to provide solid solution strengthening or, when used in conjunction with tertiary alloying additions, Mg can act as an effective precipitation strengthener of Aluminum. Its addition to Al improves corrosion resistance and weldability. Mg addition to Al lowers the modulus of elasticity of Al, and decreases its stacking fault energy (SFE). Decreasing the SFE reduces dislocation mobility, which in turn reduces the extent to which microstructural recovery can occur. Additions up to aproximately 12-14% increase hardness, strength, and fatigue resistance while simultaneously lowering density. The precipitation sequence for Al-Mg reported by Mondolfo [Ref 4: pp.311-317] is:

$$\text{Supersaturated Solution} \rightarrow \text{Al} + \beta(Mg_5Al_8)$$

A tendency for Mg to segregate to grain boundaries during precipitaion is reported. Presence of the ß phase in Al-Mg-Zr ternary systems has been

important in processing of Al-Mg-X at the Naval Postgraduate School (NPS). (See 'Previous Investigations' in this chapter)

b. Lithium

Lithium, with a density only 1/5 that of Al, is a potentially attractive alloying element for Al. It is one of the few elements that substantially reduce density while simultaneously increasing the elastic modulus of Al. Li additions to Al alloys have been observed to degrade toughness and corrosion resistance in certain circumstances. Mondolfo [Ref. 4: p. 310] and Thompson [Ref. 5] both report precipitation of a spherical, coherent, metastable δ' phase with composition $LiAl_3$ during aging of Al-Li binary alloys. Thompson [Ref. 5: pp.113,115] further reports the presence of δ' in Al-Li-Mg ternary alloys, and states the precipitation sequence as:

$$\text{Supersaturated solution} \rightarrow \delta'(LiAl_3) \rightarrow LiMgAl_2$$

where $LiMgAl_2$ is a rod-shaped dispersoid identified as the equilibrium precipitate appearing in the phase diagram [Ref. 4: p. 555].

c. Zirconium (Zr)

Zirconium is often added to commercially cast Al alloys for grain refinement which is achieved by precipitation of a fine-scale equilibrium second phase, $ZrAl_3$. The most important effect of Zr

additions to Al is that it controls the extent to which recrystallization can occur during elevated temperature processing [Ref. 6]. Inhibiting recrystallization has the effect of slowing the rate of microstructural coarsening, and this is beneficial in controlling the superplastic properties of Al alloys.

B. SUPERPLASTICITY

1. Phenomenological Considerations

No entirely satisfactory expalanation for superplasticity has yet been offered. Relationships have been proposed which are primarily phenomenological in nature and often adopt the power law behavior first proposed in 1964 by Backofen, Turner, and Avery [Ref. 7]

$$\sigma = K\dot{\epsilon}^m \qquad \text{(eqn. 2.1)}$$

where σ is the applied stress, K is a material constant, $\dot{\epsilon}$ is the strain rate, and m is a strain-rate sensitivity coefficient. The constant K is comprised of material related factors such as grain size, and diffusion coefficients which introduce a temperature dependence to SPD. The coefficient m is also material and mechanism dependent. Stress is

commonly seen to display a d^a dependence upon grain size at constant temperature and strain-rate; a is variously assigned values from 0.5 to 3.0, a=2 being typical. Conversely, strain rate may be expressed as proportional to $1/d^b$. The reccurence of this grain size dependency is an important feature of superplasticity.

Superplastic materials characteristically display high strain-rate sensitivity. That is, they show a large increase in flow stress with increasing strain rate. The strain-rate sensitivity index, m, is the slope of the log stress versus log strain-rate curve:

$$m = \frac{d(\ln \sigma)}{d(\ln \dot{\epsilon})} \qquad \text{(eq. 2.2)}$$

The stress verses strain-rate curve is constructed in the following manner. The stress-strain data for the various strain rates examined are first plotted on stress verses strain axes. Next, holding strain constant, the value of stress at that fixed strain is plotted for each strain-rate of interest. The process is then repeated for a larger value of fixed strain, and so on. The result is generally a family of curves laying one atop another, with successively higher stresses observed for larger strains. Equation 2.2

is accurate so long as equation 2.1 is obeyed, and it is the definition used throughout this thesis.

The value of m determined from experimental data, i.e. $m_{apparent} = d(\ln \sigma)/d(\ln \dot{\epsilon})$, may not reflect the underlying mechanism, i.e. m_{true} from equation 2.1, if grain size does not remain constant during deformation. The problem arises because the time required to attain a given strain varies directly with strain-rate. Consequently, tests conducted at lower strain-rates allow a significantly longer period of time for coarsening to occur. The stress at a given strain is therefore likely to be higher due to a larger grain size. The net effect is a decrease in the value of m as a function of increasing strain. For this reason, other means of determining m are commonly employed based upon change in strain-rate methods such as described by Backofen [Ref. 7].

Various theoretical models have been proposed to explain superplasticity. These fall generally into two catagories: those relying on diffusional processes, and those modeled on dislocation processes. Each has strengths and weaknesses, and none provides a thoroughly consistent explanation for all instances of SPD. Models based on established creep mechanisms are often proposed, where SPD is to be thought of as an

exaggerated form of creep. Explanations for creep commonly divide plots of stress verses strain-rate into three regions, each being dominated by a different mechanism. The existence of region I is disputed, but region II is commonly held to operate by diffusion processes, while in region III dislocation mechanisms are thought to dominate.

Examples of diffusional processes include Herring-Nabarro creep, which relies on bulk diffusion of vacancies from grain interiors to grain boundaries to produce grain elongations, and Coble creep which operates by grain boundary diffusion of vacancies resulting in grain boundary sliding. More explicit grain boundary sliding models exist. The Ashby-Verrall model explains SPD as a process of grain boundary sliding accomodated by diffusion. More recently, Ruano and Sherby [Ref. 8] have shown that results more consistent with reported data are obtained by modeling SPD as grain boundary sliding accomodated by slip. Certain dislocation creep models have been proposed to account for superplastic behavior. Orowan [Ref. 9] explained creep as the competition between rate of hardening due to plastic strain, and rate of recovery due to exposure to high temperatures. Weertman offered an explanation for creep that relies upon dislocation climb to overcome obstacles which would otherwise prevent further elongation [Ref. 10].

One of the factors complicating these characterizations of superplasticity is the likelihood that a number of mechanisms may operate simultanesously during deformation. While superplastic deformation at lower strain-rates manifests the $1/d^b$ grain size dependence mentioned earlier, at higher strain rates dislocation mechanisms begin to dominate. This has lead to expressions for SPD of the form

$$\dot{\epsilon} = K_1 \frac{D_{eff} b}{d^p} \left[\frac{\sigma}{E}\right]^{1/m} + K_2 D_s \sigma^3 \qquad \text{(eq. 2.3)}$$

where K_1 and K_2 are constants, D_{eff} is the effective diffusion coefficient, b is the burgers vector, β is the applied stress, d is the grain size, p the grain size exponent, E is the elastic modulus, m is the strain-rate sensitivity coefficient, and D_s is the diffusion coefficient for solute diffusion. This equation is constructed from two empirical relationships. The first term was proposed by Ruano and Sherby [Ref. 8: p. 171] to describe the region II behavior of SPD. The second term, attributable to Weertman [Ref. 11], describes region III behavior where dislocation processes are thought to dominate.

2. Microstructural Considerations

It is widely accepted that superplastic behavior requires an equiaxed grain structure of uniformly fine grain size, typically less than 10 microns, and a strain rate consistent with $m \geq 0.3$. Such a microstructure is most commonly produced by mechanical working of the material. SPD typically requires temperatures equal to or greater than $0.4T_m$, where T_m is the absolute melting temperature of the alloy. Such temperatures are necessary for activation of the diffusion and dislocation mechanisms believed responsible for superplasticiy. Often, however, rapid microstructural coarsening also occurs at these temperatures. Clearly then, some form of grain refinement is necessary if the elevated temperature – fine grain size requirements for SPD are to be met simultaneously. This leads necessarily to a consideration of the recovery and recrystallization mechanisms operative at these temperatures.

a. Recovery

Recovery refers to the process whereby dislocation networks introduced during mechanical working rearrange themselves into lower energy configurations without recrystallization or change in orientation of the crystal lattice. Such rearrangement is termed polygonization when

recovery results in a rearrangement of the dislocations into cellular arrays [Ref. 12]. The driving force for recovery is reduction of the large amount of stored energy introduced during working.

b. Recrystallization

Recrystallization following recovery is observed to occur by two distinct modes. The term "discontinuous" recrystallization has been used to describe the process of nucleation and growth of new, strain-free grains into the surrounding deformed crystal lattice along a well defined reaction front. In the absence of any retarding influence, growth of the strain-free grains continues unrestricted. The large grain size that results raises flow stress rapidly and halts SPD. Discontinuously recrystallized microstructures are generally unsuitable for SPD. "Continuous" recrystallization does not occur by nucleation and growth but rather by the gradual migration and coalesence of subgrains, resulting in formation of high-angle grain boundaries [Ref. 13]. These high-angle boundaries are generally quite stable and resistant to coarsening. Hence, if a fine initial grain-size can be established it may be expected to exhibit good microstructural stability, coarsening little with time. Continuous recrystallization seems capable, therefore, of reconciling the

competing requirements of fine grain size and elevated temperatures necessary for SPD.

McQueen and Jonas [Ref. 14: pp. 396-401] have proposed a recovery and recrystallization model for metals with high stacking fault energy which may be of particular significance in the present alloys. Their model includes the following sequence of events:

1. Development of a cellular dislocation substructure as strain increases during cold working.
2. Recovery during annealing by annihilation of dislocations and formation of subgrain boundaries.
3. Establishment of an equilibrium size which remains constant during steady state flow.
4. Coalesence of adjacent cells to form a crystallite nucleus. This occurs by movement of dislocations to surrounding subboundaries increasing subboundary misorientation until they are able to migrate freely.

3. Previous Investigations

Previous work at Naval Postgraduate School has centered on the Al-Mg-X system where response to high Mg concentrations during thermomechanical processing and subsequent SPD has been the focus of special interest.

Three recent investigations are of particular importance. Self [Ref. 15] examined the effect of Cu and Mn additions to 8%Mg and 10%Mg, Al-Mg

alloys. This work included examination of warm temperature mechanical properties and demonstrated that, regardless of tertiary alloy concentration, higher ductilities were obtained as Mg content increased. Berthold [Ref. 16] and Alcamo [Ref. 17] worked concurrently to establish the microstructural characteristics and mechanical properties during warm temperature deformation of an Al-10%Mg-0.1%Zr alloy warm rolled to 94% reduction. Both studies included TEM micrographs of the alloy in the as-rolled, statically annealed, and SPD conditions. Continuous recrystallization and superplastic behavior was observed at temperatures just below the solvus for Mg. Recrystallization accompanied by extensive cavitation during deformation of the material was observed for tensile tests conducted at temperatures above the solvus. Self and Alcamo both report a decrease in flow stress, and an increase in the strain-rate sensitivity coefficient, m, with increasing Mg concentration. Such findings are consistent with work by McNelley and Garg [Ref. 18] which demonstrated that thermomechanical processing at temperatures just below the solvus for Mg in Al-10.2%Mg reduced the Mg in solution to roughly the solubility limit of Mg in Al at the processing temperature. It is not unreasonable, therefore, to expect that increasing Mg content will produce a corresponding

increase in volume fraction of second phase ß precipitated. Self [Ref. 15: p. 55] and Alcamo [Ref. 17: p. 50] both suggested that increased precipitation of intermetallic ß exerted a rerfining effect on grain size.

With regard to stability of the microstructre, Berthold [Ref. 16: pp. 54, 81] and Alcamo [Ref. 17: pp. 72-73] reported no discernable coarsening of the microstructure after initial recovery and recrystallization had occurred in specimens subjected to isothermal annealing only. Stable grain size was reported within the first 60 minutes of annealing. In specimens undergoing SPD, however, grain growth was observed. One may infer from such evidence that the growth mechanism in these thermomechanically processed alloys may be diffusion controlled process which is accelerated by deformation.

The present thesis seeks to extend the knowledge gained in these past observations to an understanding of the Al-Mg-Li-X system, and to determine whether similar behavior is to be expected.

III. EXPERIMENTAL

A. MATERIAL PROCESSING AND MICROSTRUCTURAL DEVELOPMENT

The nominal composition of the two alloys in weight percent was reported to be Al-8%Mg-0.5%Li-0.15%Zr and Al-8%Mg-1.0%Li-0.15%Zr [Ref. 19]. Independent verification of the Mg, Li, and Zr concentrations was performed by atomic absorbtion and x-ray techniques for the 0.5%Li alloy.

1. Thermomechanical Processing

The alloys were received as cast ingots 7 inches in height with a 4 inch maximum diameter at the base. These ingots were cast by the Naval Surface Weapons Center (NSWC), White Oak, Maryland. The ingots were first halved, and each half was then quartered into 4 billets. Each billet was solution treated 5 hours at 440°C followed by an additional 19 hours at 480°C to re-solution any Mg or Li containing second phases. The billets were hot worked to a 3:1 reduction by upset forging on heated plattens, and then returned to the 480°C furnace for an additionl 60 minutes before being oil quenched. Each billet was then isothermally deformed at 300°C by warm rolling to a final reduction of 85% (true strain = -1.9) with reheating

between passes. The reduction per pass was 0.04 inches (1.0 mm). On completion of rolling, the specimens were vigorously oil quenched. A schematic representation of the thermomechanical process is presented in Figure 1.

2. Specimen Geometry

Two specimen geometries were employed. The ambient temperature test specimens were prepared as described by Klankowski [Ref. 20]. The overall dimensions measured 2.9 in. in length x 0.5 in. in width with a gage section of 1.0 in. in length x 0.25 in. in width. A tapered shoulder with radius of curvature 0.5 in. was used to transition from the gage to the grip sections.

The elevated temperature test specimens were prepared with the geometry described by Alcamo [Ref. 17: pp. 36-37]. Overall dimensions of 2.5 in. in length x 0.5 in. in width with a gage section of 0.5 in. in length x 0.2 in. in width. An abrupt shoulder with radius of curvature equal to 0.0625 in. was used as the transition from gage to shoulder sections.

B. TENSILE TESTING

All tensile tests were performed on an Instron Model TT-D. Ambient temperature specimens were held by wedge grips and strained until fracture

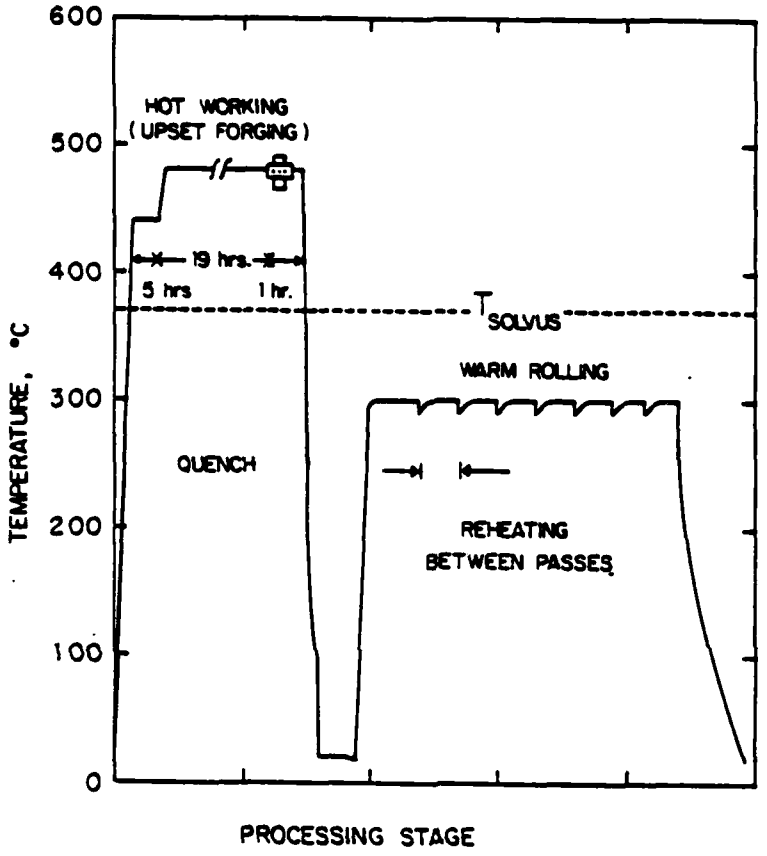

Figure 1. Schematic Representation of the Thermomechanical Process.

at a constant strain rate of $8.3 \times 10^{-4}\ s^{-1}$. The elevated temperature test apparatus was the same as employed by Self [Ref. 15: pp. 31-33] and Alcamo [Ref. 17: pp.38-40], a Marshall 2232 three zone clamshell furnace. Thermocouple placement within the furnace was designed to assure temperature uniformity with position and time. Crosshead speeds ranged from 0.002 in./min. to 5 in./min. producing a corresponding variation in strain-rate of $6.7 \times 10^{-5}\ s^{-1}$ to $1.7 \times 10^{-1}\ s^{-1}$.

C. DATA REDUCTION

1. Equations Used

The following definitions and terms were used in calculating the values reported throughout this paper:

$$S = \frac{F}{A_0} \qquad \text{Engineering Stress}$$

$$e = \frac{L_f - L_0}{L_0} \qquad \text{Engineering Strain}$$

$$\sigma = S(1 + e) \qquad \text{True Stress}$$

$$\epsilon = \ln(1 + e) \qquad \text{True Strain}$$

These latter two equations are only valid prior to the onset of necking.

2. Discrepencies Between Charted and Measured Strain

Differences between the chart-predicted strain and that measured from the gage marks of SPD specimens occured in all tests. This was attributed to grip seating, tension rod alignment, and other such unquantifiable variables. In order to predict as accurately as possible the true elongations from the charted values, a scale factor equal to the ratio of the measured elongation at fracture to the chart-predicted value at fracture was applied to each data point of a given test. Hence, at fracture the two values coincide exactly.

D. METALLOGRAPHY

1. Optical Microscopy

Specimens were first mechanically ground and polished to a planar, scratch free surface by standard metallographic techniques [Ref. 21]. Following this they were electrolytically polished to remove the final traces of mechanical disturbance from the surface. The specimens were submerged in a solution of 20% HNO_3 in methanol and connected as the anode across a constant 10 vdc potential. Liquid Nitrogen was used to reduce the temperature of the electrolyte to 0°C, thereby slowing the reaction rate to

manageable times. Polishing times varied from $^1/_4$ - 1 second depending upon the degree of warm working received, the more highly worked specimens requiring less time.

Following elecrolytic poslishing, the specimens were anodically etched to produce a surface coating suitable for examination of microstructural details in cross-polarized illumination conditions. The electrolyte employed was composed of:

34.6 ml of HF acid

13.6 gm of Boric acid

Distilled water sufficient to make up solution to 1000 ml.

The specimens were submerged, connected anodically across a 10 vdc potential, and etched from 1-5 seconds, the time again depending upon degree of warm working.

2. Transmission Electron Microscopy

Blanks of 50µm thickness were sectioned parallel to the long transverse plane of both superplastically deformed and as-rolled specimens. The blanks were then reduced to c. 35µm thickness by mechanical grinding on fine-grit silicon carbide papers. Reduction to a final thickness of 25-30µm was achieved by caustic etching at 60°C in NaOH to remove any

mechanical distortion from the surface. Each blank was given a final surface cleaning in a solution of 30% HNO_3 in methanol, and rinsed under tap water. Thin foil specimens of 3mm disc size were prepared with a Struers polisher utilizing 20% HNO_3 in methanol as the electrolyte. The electrolyte temperature was reduced to -20°C, and a potential of 15 vdc was applied. Thin foil specimens were examined in a JEOL (JEM-100 CX II) transmission electron microscope.

IV. RESULTS

A. ALLOY COMPOSITION

Results of the detailed chemical analysis performed by atomic absorbtion and x-ray techniques for the Al-8.0%Mg-0.5%Li-0.15%Zr alloy are listed in Table I [Ref. 22].

TABLE I. CHEMICAL ANALYSIS FOR AL-MG-LI-ZR ALLOY

	Element(wt.%)			
Position*	Mg	Li	Zr	Al
1 (Surface)	8.12	0.53	0.23	Balance
2	8.26	0.49	0.23	Balance
3	7.95	0.49	0.23	Balance
4	7.71	0.47	0.23	Balance
5 (Center)	7.44	0.47	0.25	Balance

* The five samples were of equal dimension, and were about equally spaced along a radius from the surface to the center of the ingot.

Compositional uniformity of the Al-8.0%Mg-1.0%Li-0.15%Zr alloy was assumed to be similar, therefore no comparable chemical analysis was performed.

B. MICROSTRUCTURAL DEVELOPMENT

1. Optical Microscopy

Development of the microstructure during thermomechanical processing is presented in Figures 2 through 4. The as-cast microstructure is clearly dendritic (Fig. 2a) with porosity and segregation of eutectic *microconstituent to grain boundaries and inter-dendrite spaces in evidence.* Solution treatment and hot work by upset forging transformed the microstructure to a homogeneous, equiaxed, and strain-free condition (Fig. 2b). *Large changes in contrast across the specimen surface indicate that a* high degree of misorientation exists across grain boundaries. This micrograph shows that a fully recrystallized microstructure has been *produced at the high temperatures of solution treatment. There is no* evidence of second phase precipitates remaining on grain boundaries or in grain interiors, indicating that all Mg has returned to solution. Progressive grain elongation with increasing precipitation of second phases has occured

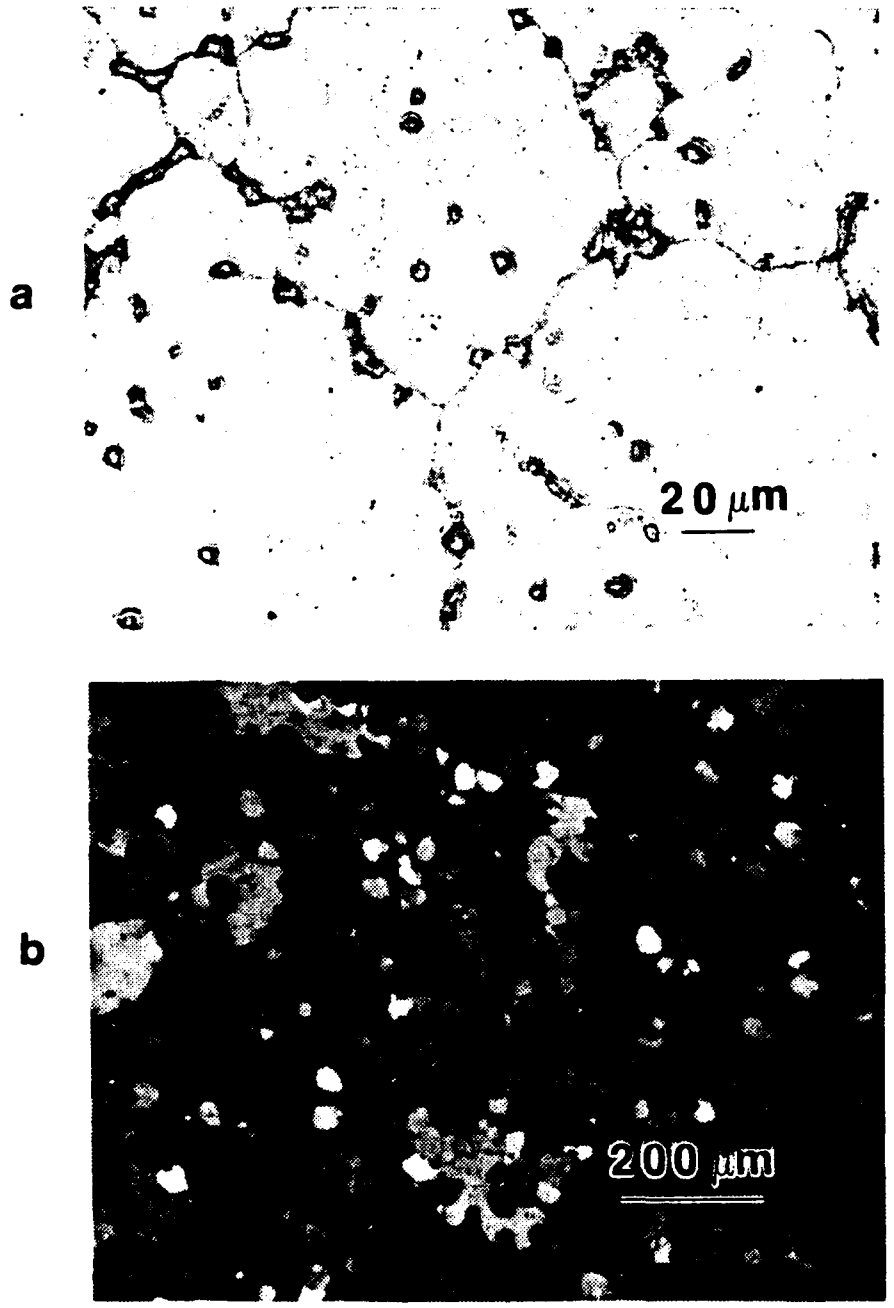

Figure 2. Evolution of Microstructure in Al-8.0%Mg-0.5%Li-0.15%Zr. Optical micrographs of (a) the dendritic as-cast microstructure, and (b) the solution treated and hot worked microstructure using cross-polarized illumination. Solution treating and hot work has produced a fully homogenized, equiaxed, strain-free microstructure.

during warm rolling. Figures 3 and 4 show the microstructural refinement achieved during warm rolling of these alloys. The initial grain boundary decoration by precipitated second phase(s) has been gradually replaced by an increasingly homogeneous microstructure as the thermomechanical treatment progressed.

2. Transmission Electron Microscopy

Microstructural examination of as-rolled specimens using TEM showed a steady increase in dislocation density with increased rolling strain (Figs. 5, 6, 7). Each bright field-dark field pair in Figures 5, 6, and 7 corresponds to one of the rolling reductions seen in Figures 3 and 4. By the completion of warm rolling (85% reduction), grain boundaries had become indistinguishable. Precipitation of second phases during warm rolling was clearly visible by the time a 47% reduction had been achieved. Thereafter only increases in dislocation density accompanied by refinement of precipitates was discernable. The high degree of mechanical working in the material is also evident in the faulted appearance of the precipitates. This faulting was no longer discernable for individual precipitates in the final rolled condition.

Examination of superplastically deformed specimens shows clear evidence of microstructural coarsening with time and strain during

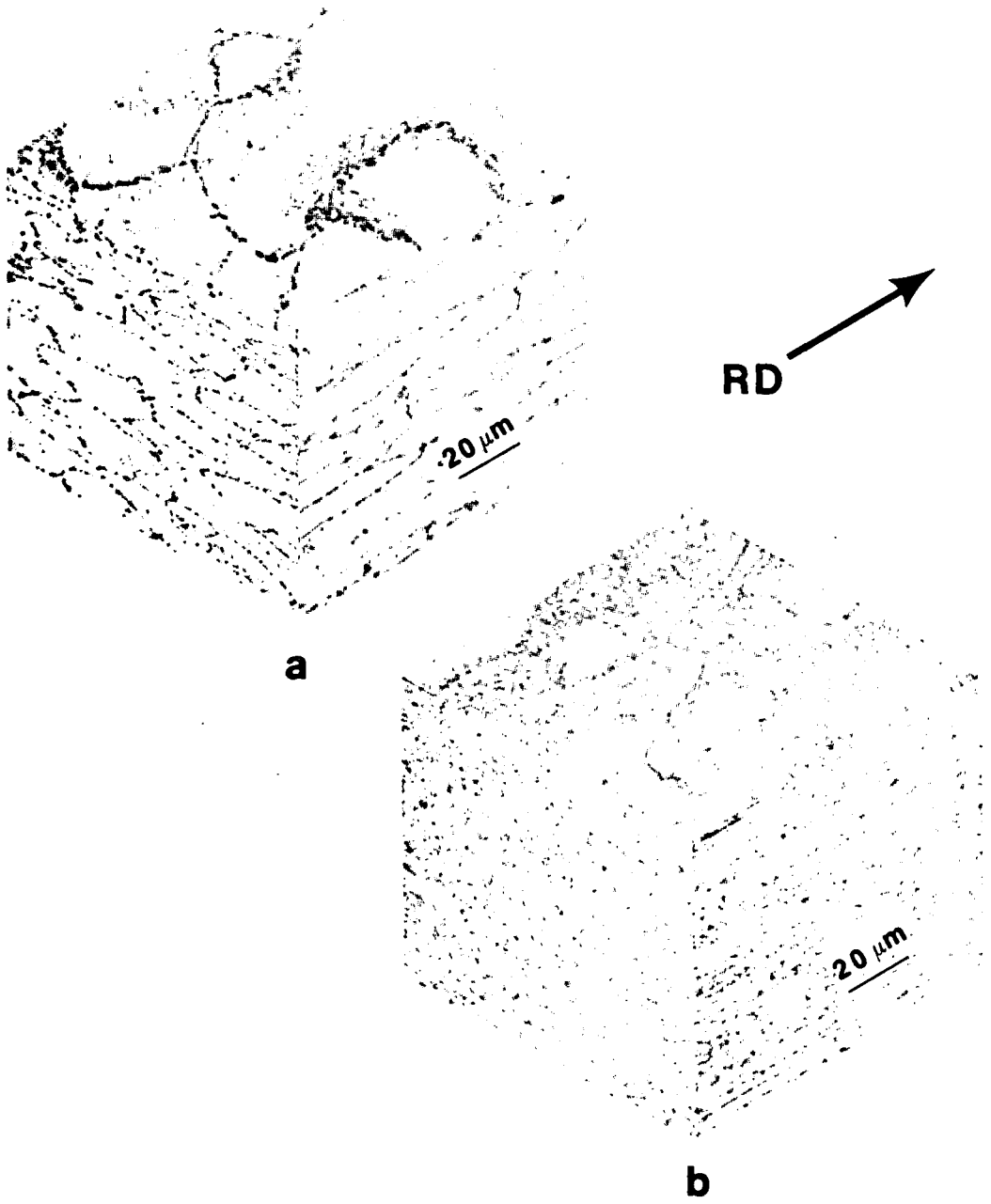

Figure 3. Triplanar Micrographs of Al-8.0%Mg-0.5%Li-0.15%Zr Alloy. Two intermediate rolling stages are shown: a rolling reduction of 47% (a) showing grain elongation, and grain boundary decoration by precipitates, and (b) a rolling reduction of 77% showing increasing elongation, and precipitation within grain interiors.

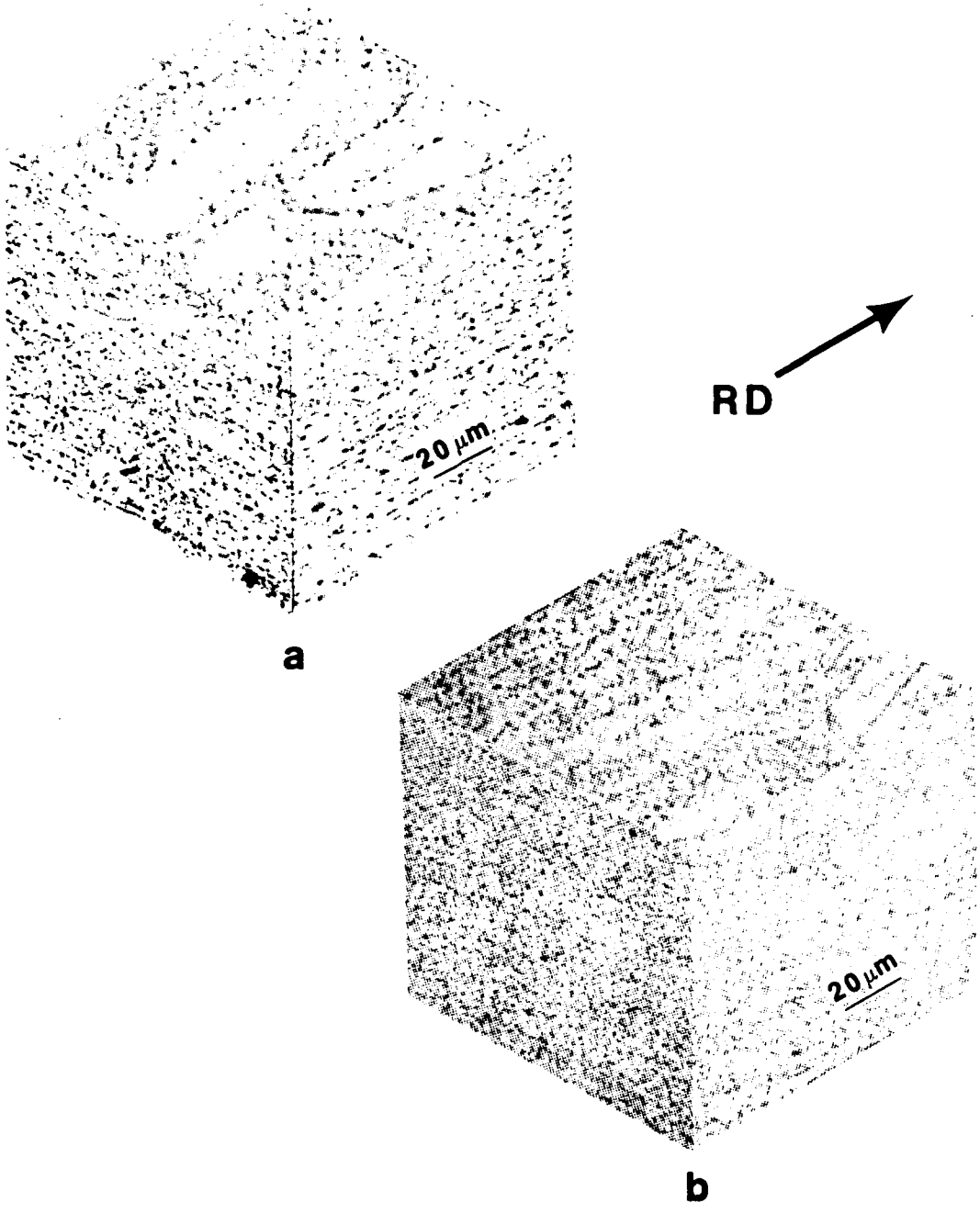

Figure 4. Final As-Rolled Microstructure (85% Reduction) for (a) Al-8.0%Mg-0.5%Li-0.15%Zr Alloy and (b) Al-8.0%Mg-1.0%Li-0.15%Zr Alloy. Both alloys show the high degree of microstructural refinement achieved by thermomechanical processing.

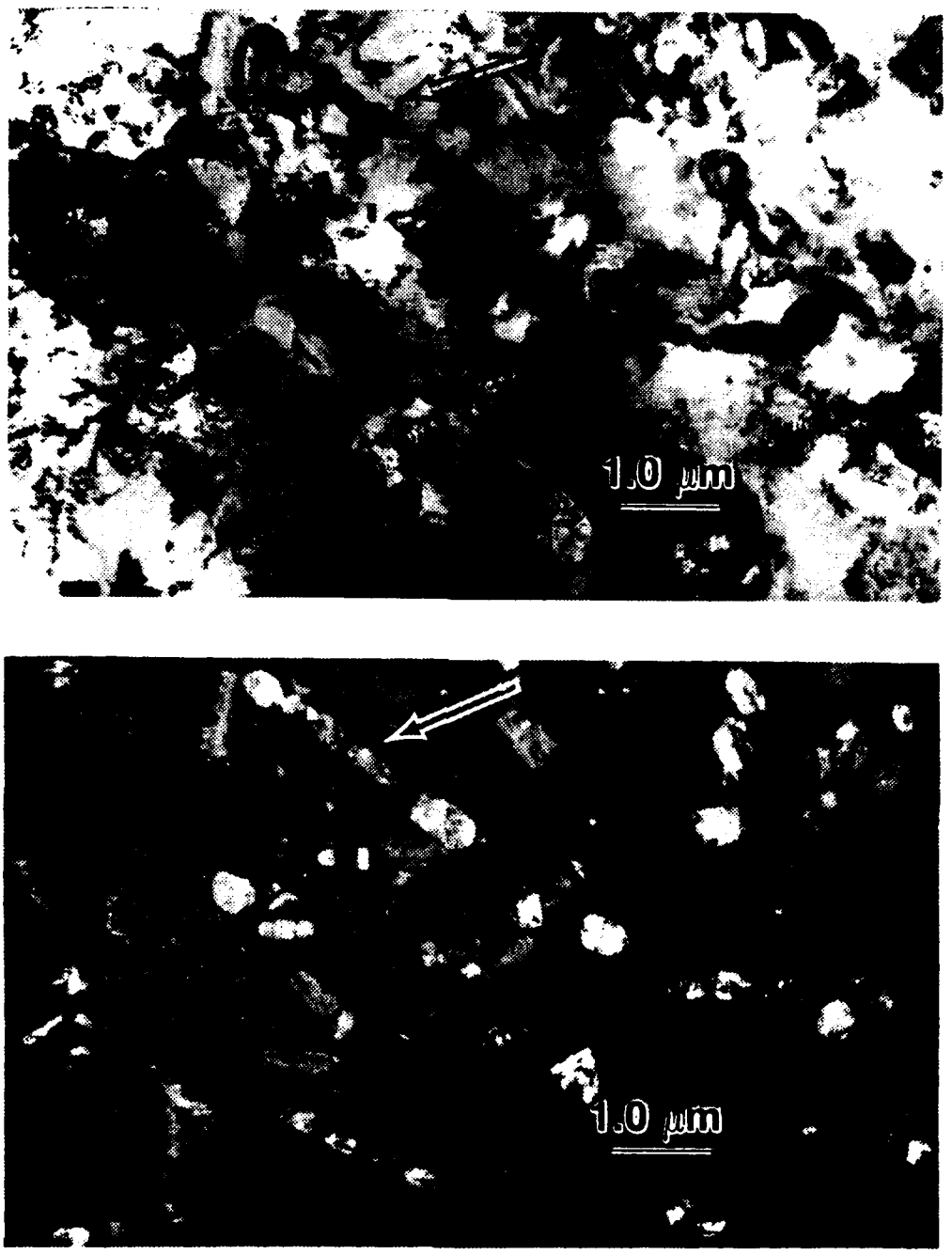

Figure 5. TEM Micrographs of Al-8.0%Mg-0.5%Li-0.15%Zr at 47% Rolling Reduction Showing Precipitation of Second Phase Particles and the High Dislocation Density Generated by Warm Rolling. ß-phase clearly visible on grain boundary (arrow). Bright field (a). Dark field (b).

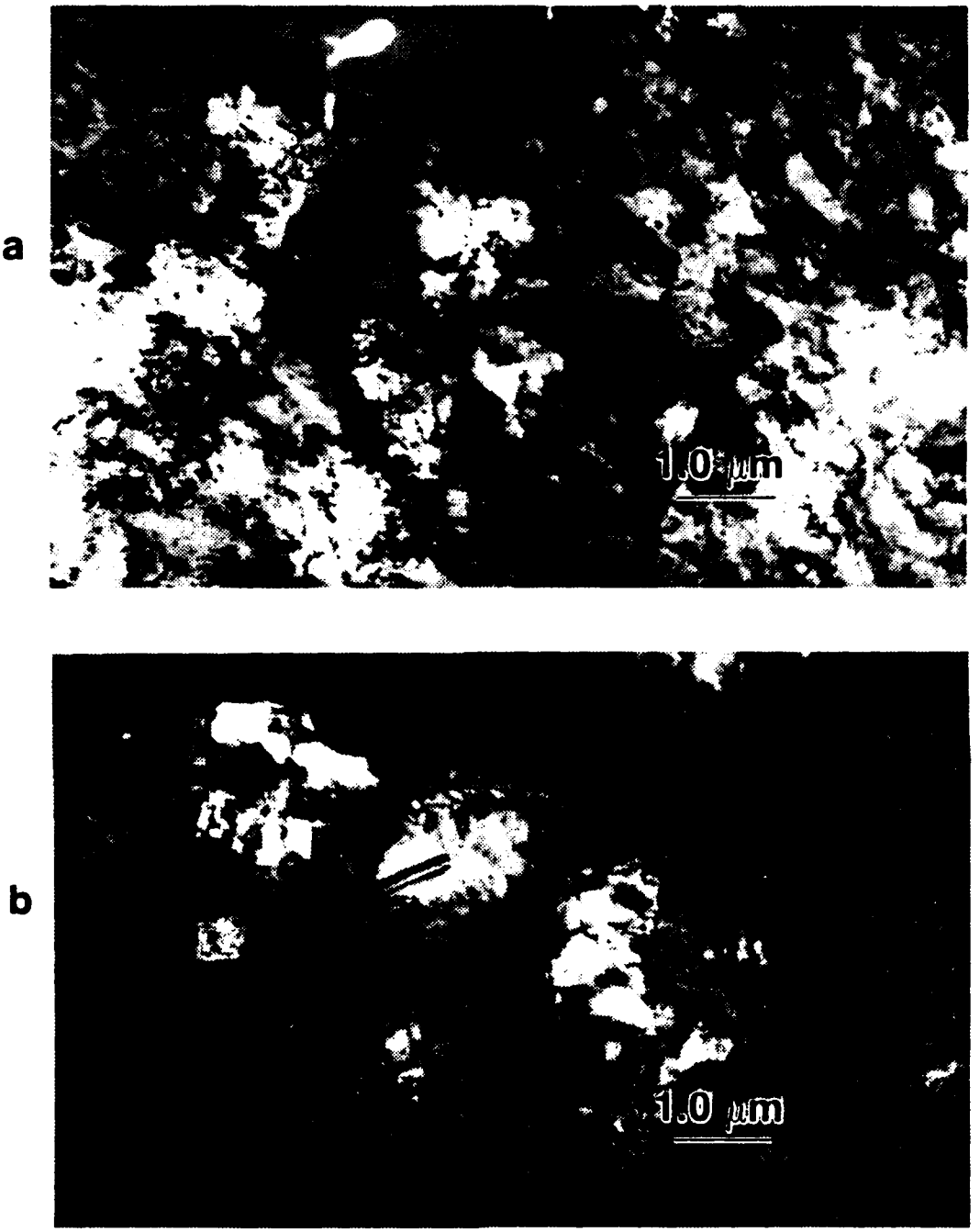

Figure 6. TEM Micrographs of Al-8.0%Mg-0.5%Li-0.15%Zr at 77% Rolling Reduction Showing Increased Dislocation Density. Bright field (a). Dark field (b).

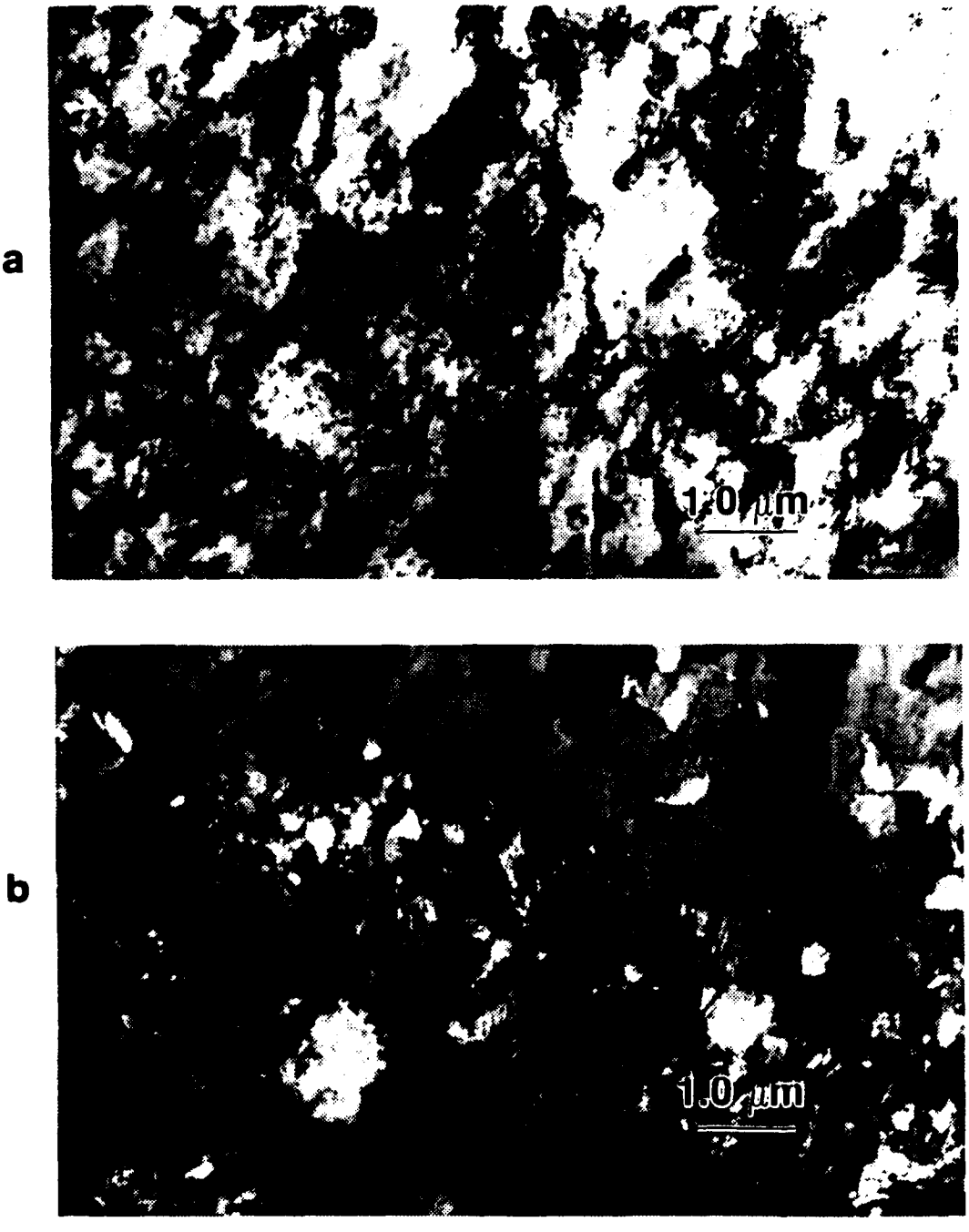

Figure 7. TEM Micrographs of Al-8.0%Mg-0.5%Li-0.15%Zr at 85% Final Rolling Reduction Showing Extreme Refinement of the Microstructure. Bright field (a). Dark field (b).

subsequent elevated temperature deformation (Figs. 8, 9). High- and low-angle boundaries were visible in all SPD specimens, with the number of low-angle boundaries decreasing with increasing test duration. Three distinct precipitate morphologies were observed (Fig. 10). These include large, irregular precipitates often found on grain boundaries; smaller, approximately spheroidal particles within grains; and a fine, coherent precipitate also seen in grain interiors. Selected area diffracation patterns (SADP) positively identified the large, irregular precipitates as ß-phase (Mg_5Al_8), and the fine, coherent precipitates as the metastable δ' phase ($LiAl_3$) [Ref. 23]. Attempts to identify the approximately spheroidal particles were unsuccessful.

C. AMBIENT TEMPERATURE PROPERTIES

A decline in strength, and a small reduction in ductility occured when Li concentration increased (Fig. 11). This is confirmed by comparison of the data in Tables II and III (See Appendix).

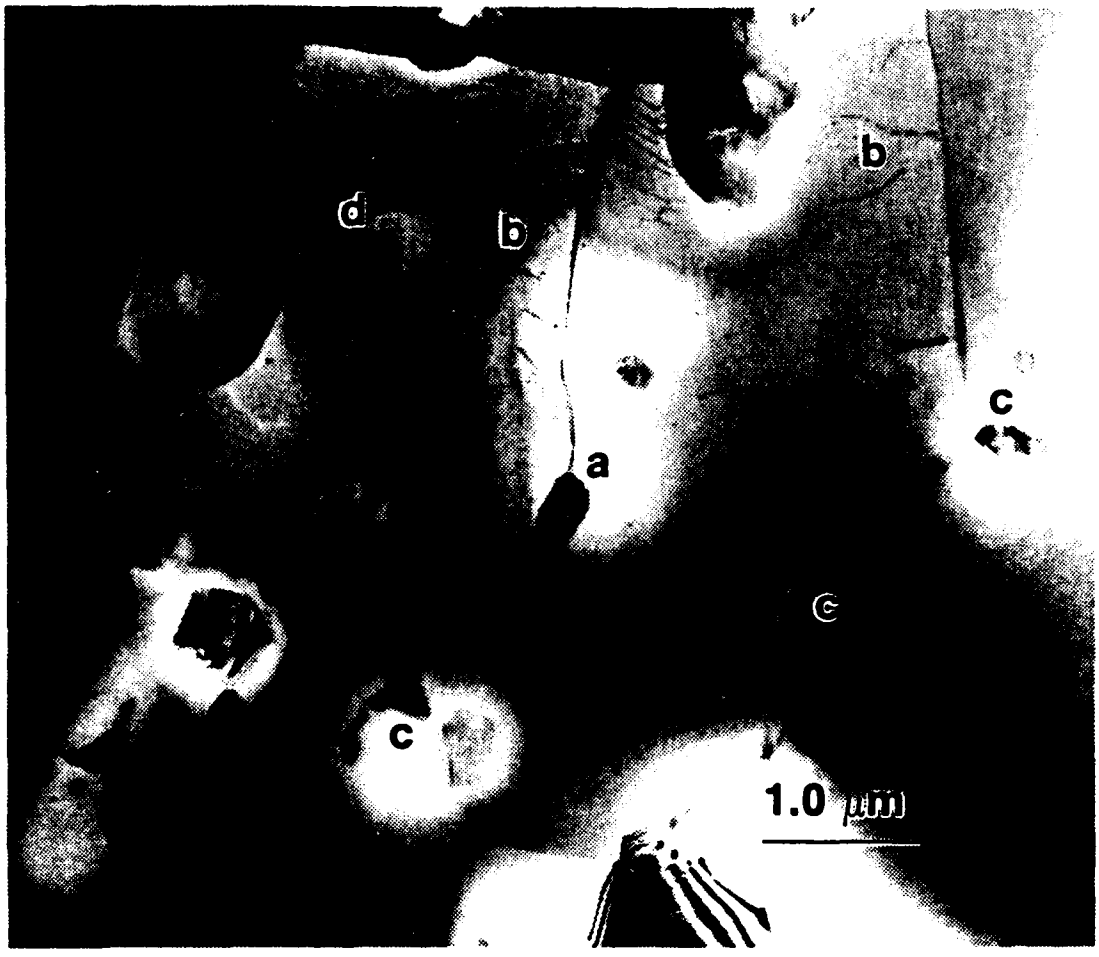

Figure 8. TEM Micrograph of Al-8.0%Mg-1.0%Li-0.15%Zr After SPD at Strain Rate $6.7 \times 10^{-4}\ s^{-1}$. Evidence for continuous recrystalization is seen by interaction of migrating subgrain boundry with spheroidal precipitate (a); interaction of individual dislocations with fine dispersoid $LiAl_3$ particles (b); β-phase precipitate pinning grain boundary (c). A dislocation network, possibly just released from the spheroidal precipitate in subgrain interior, is visible at (d).

Figure 9. TEM Micrograph of Al-6.0%Mg-1.0%Li-0.15%Zr After SPD at Strain Rate 6.7 x 10^{-5} s^{-1} Demonstrating Grain Coarsening in These Alloys. Microstructural features include interaction of individual dislocations with fine dispersoid $LiAl_3$ particles (a); pinning of grain boundary by ß-phase precipitate; spheroidal precipitates in grain interior (c). Subgrain boundaries noticeably absent.

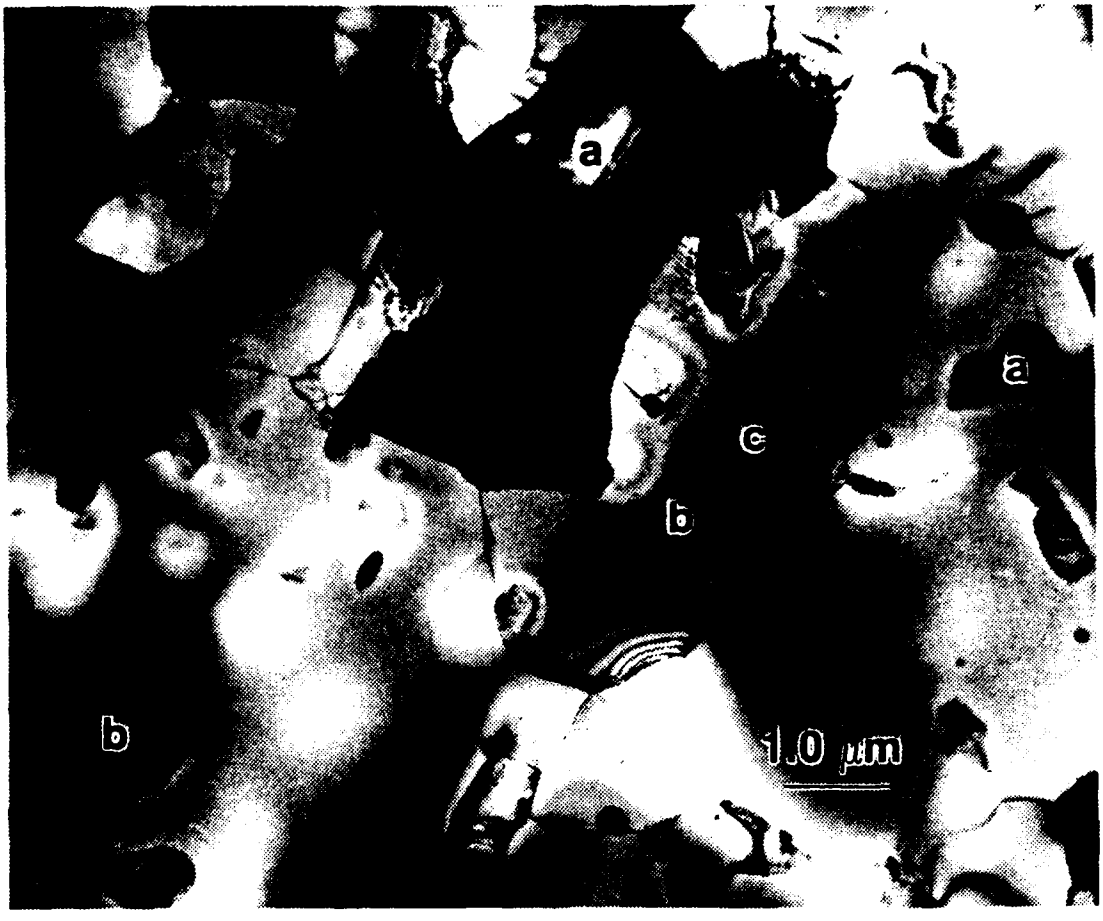

Figure 10. TEM Micrograph of Al-8.0%Mg-1.0%Li-0.15%Zr Showing Three Distinct Precipitate Morphologies: Large, Irregular Precipitate (a); Large, Approximately Spheroidal Precipitate (b); Fine, Spheroidal Precipitate (c).

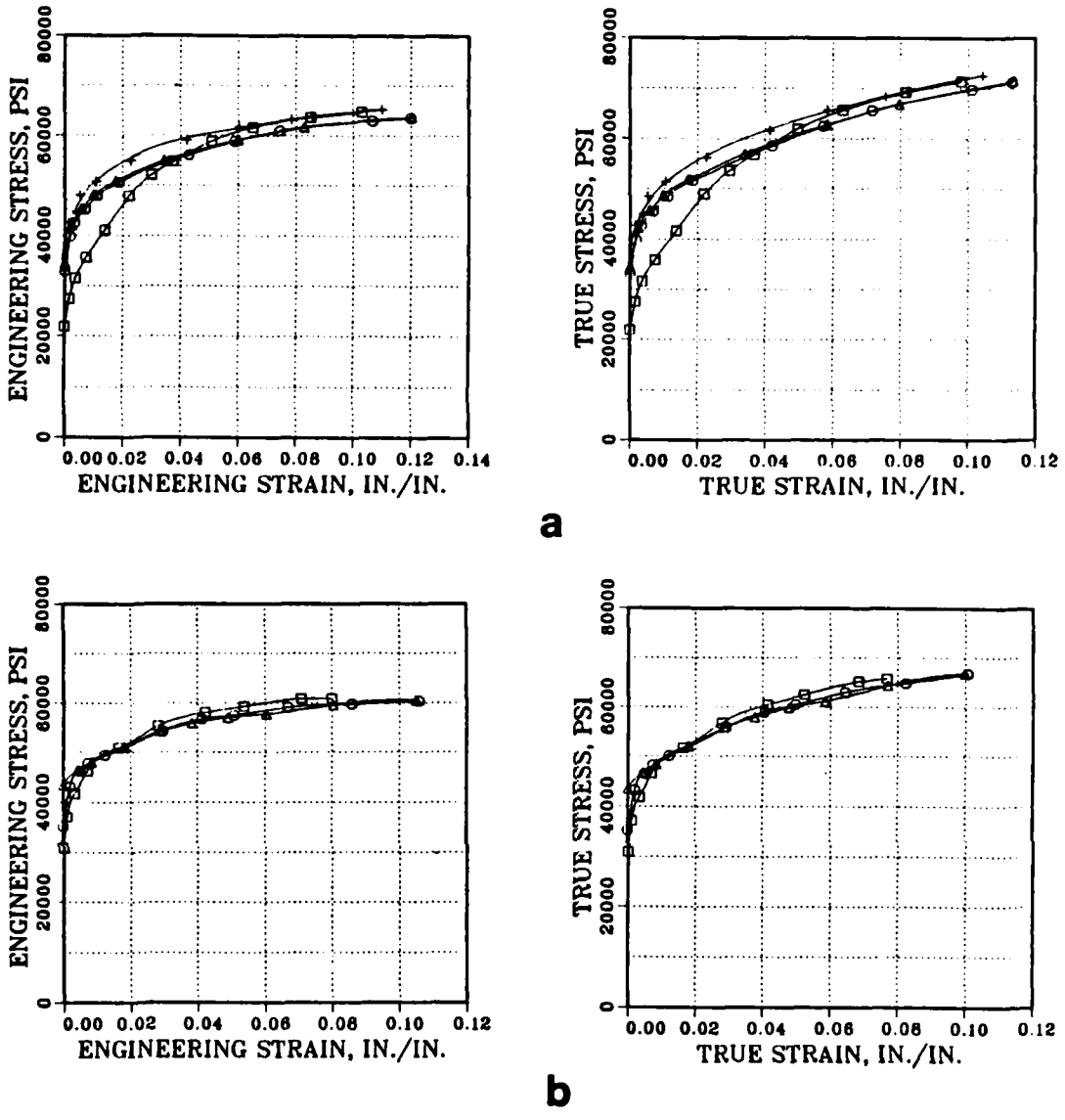

Figure 11. Ambient Temperature Tensile Test Data for (a) Al-8.0%Mg-0.5%Li-0.15%Zr and (b) Al-8.0%Mg-1.0%Li-0.15%Zr at 20°C Showing a Decrease in Strength with Increase in Li Concentration.

D. ELEVATED TEMPERATURE PROPERTIES

Strength was observed to decline with increases in Li concentration at elevated temperatures (Fig. 12) but, in contrast to room temperature behavior, Figure 13 and Table II and III all show a rise in ductility for increased Li content. The increase in Li concentration from 0.5 to 1.0wt.% appears to produce a beneficial effect on ductility at the highest and lowest strain-rates; the effect on moderate strain-rates is more ambiguous (Fig. 13a). The increase in Li concentration also produced a reduction in flow stress, with a corresponding increase in the strain rate sensitivity coefficient from approximately 0.25 to 0.3 (Fig. 13b). This effect may also be seen in the family of curves generated when true stress verses strain rate at variety of fixed strains is plotted from the data obtained during SPD (Fig. 14).

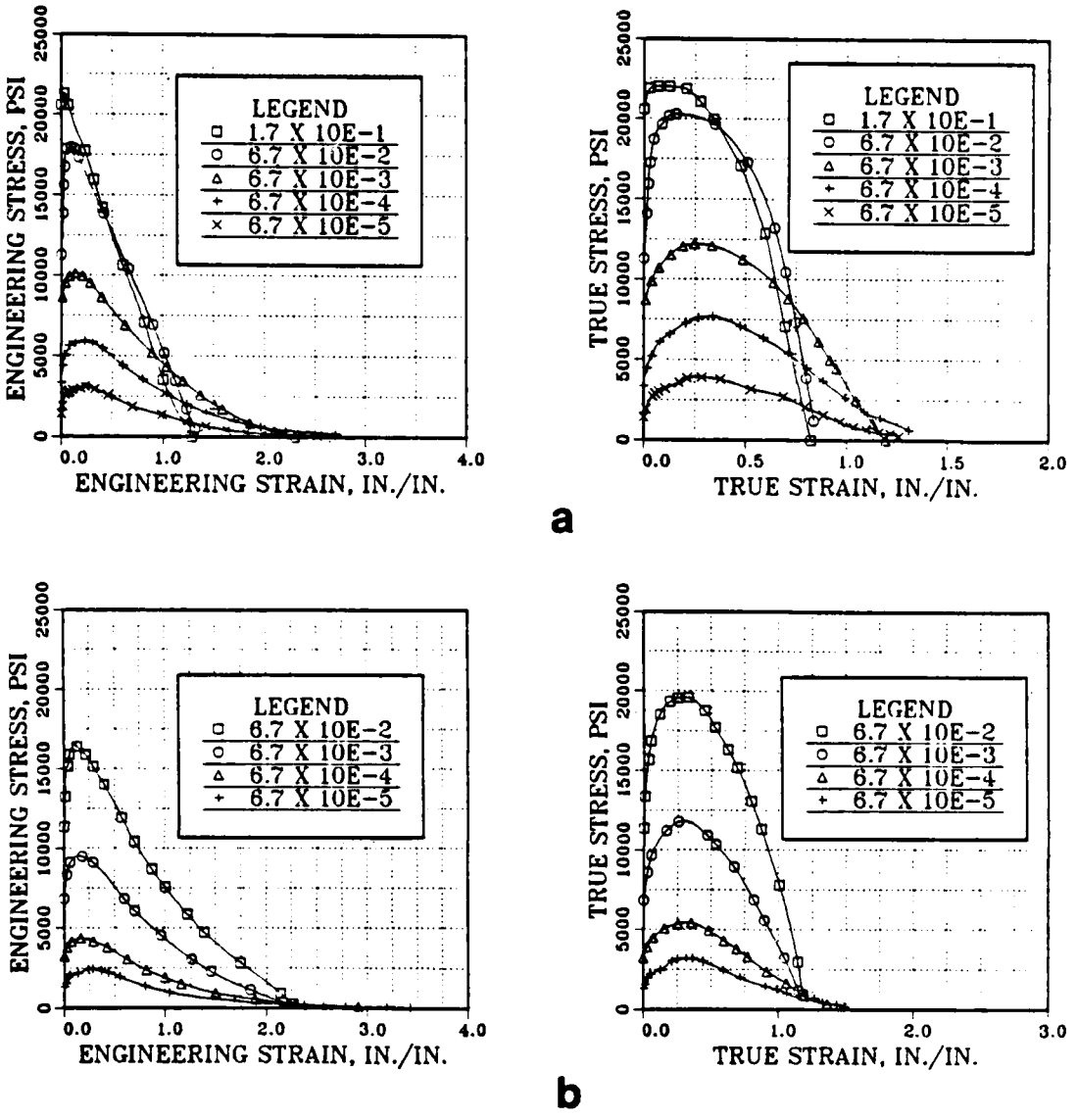

Figure 12. Elevated Temperature Tensile Test Data for (a) Al-8.0%Mg-0.5%Li-0.15%Zr and (b) Al-8.0%Mg-1.0%Li-0.15%Zr Superplastically Deformed at 300°C. Strain rates as indicated. Strength decreased but ductility increased with increased Li content.

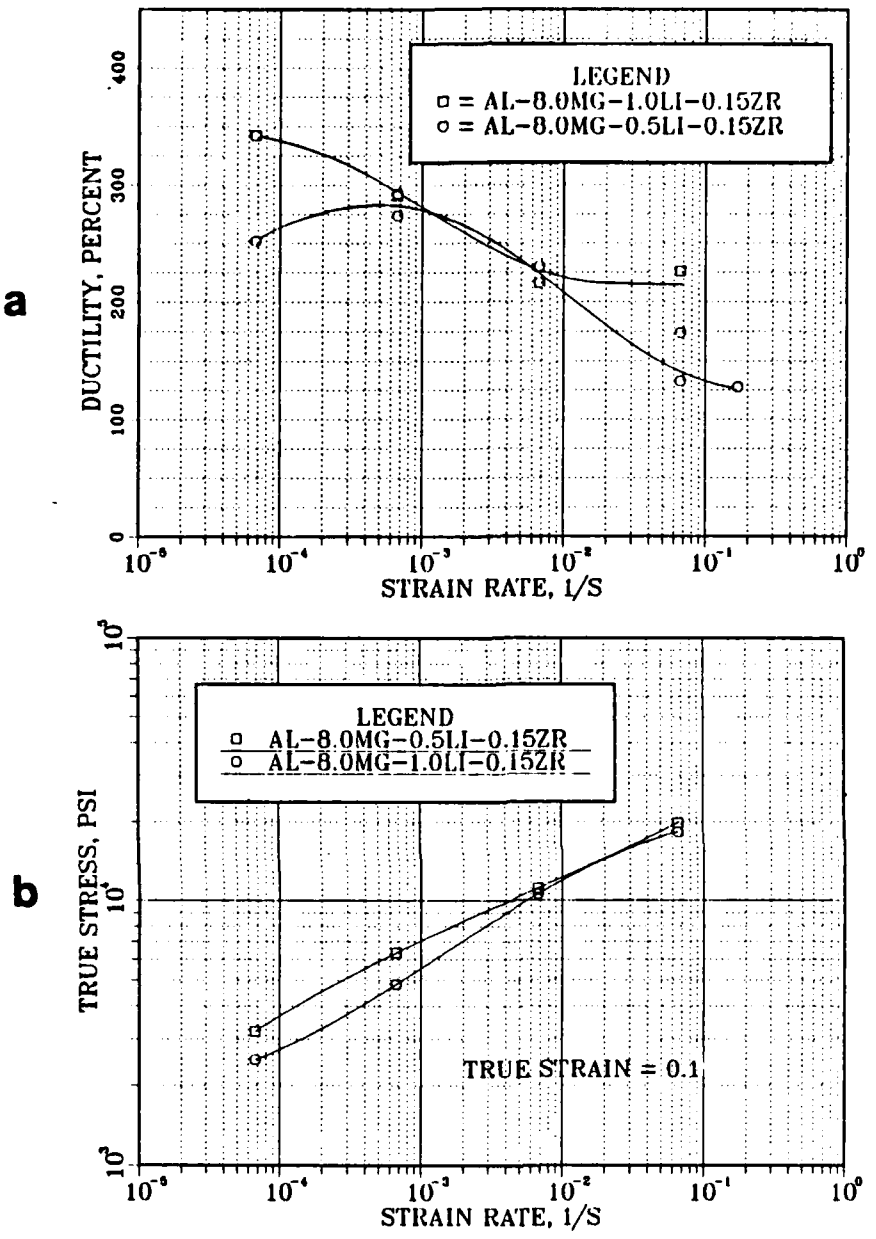

Figure 13. Percent Ductility Versus Strain Rate for Elevated Temperature Tests at 300°C (a). Both alloys demonstrate moderate superplasticity. The higher ductility of the 1.0%Li alloy is consistent with its larger m value and lower flow stress (b).

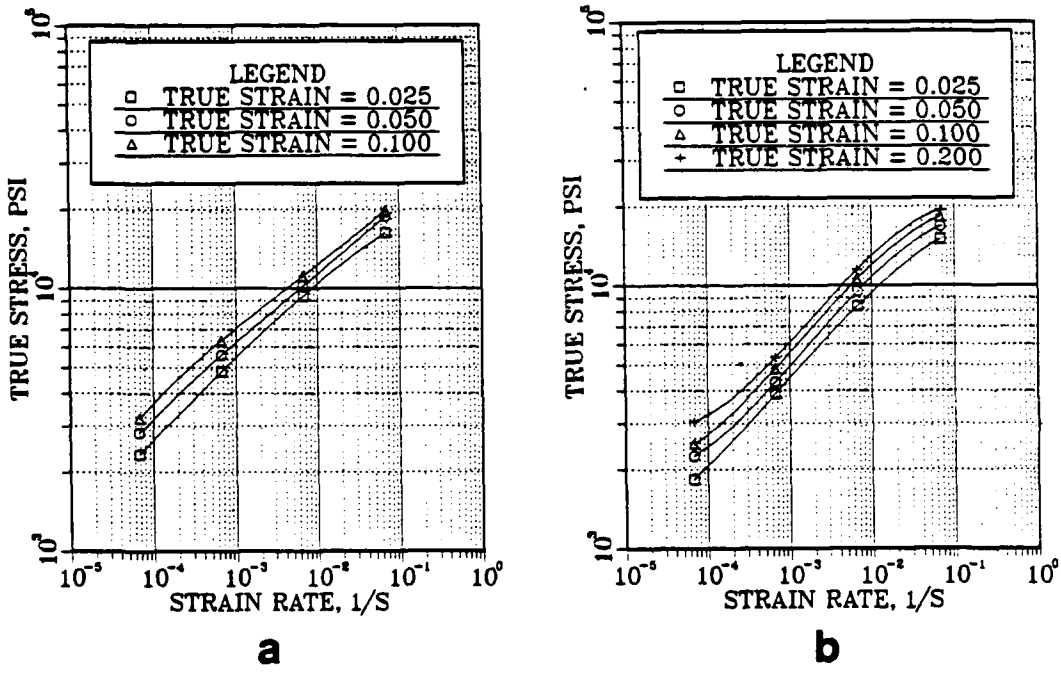

Figure 14. True Stress Versus Strain Rate at Selected Fixed Strains. The values of m vary from m≈0.25 for Al-8.0%Mg-0.5%Li-0.15%Zr (a), to m≈0.31 for Al-8.0%Mg-1.0%Li-0.15%Zr (b). The data indicates a nearly constant rate of strain hardening in both alloys.

V. DISCUSSION

A. SIMILARITIES TO PREVIOUSLY STUDIED AL-MG-X ALLOYS

1. Effect of Mg Content

Comparison of Figures 3 and 4 with the triplanar micrographs reported by Self [Ref.15: pp. 38-39,41,43,45] and Berthold [Ref.16: p. 46] reveal the similarities between these alloys and those Al-Mg-X compositions previously studied at NPS. A comparison of Figures 5, 6, and 7 with the TEM micrographs of Berthold [Ref.16: pp. 59,82,84] and Alcamo [Ref. 17: pp. 76-80] provides further evidence that the Li-containing alloys respond to thermomechanical processing and SPD in a manner strikingly similar to the earlier Al-Mg-X alloys. Additionally, the strength-ductility combinations seen in the Li alloys are comparable to those of past binary and ternary Al-Mg compositions studied at NPS (Tables II,III,IV,V of Appendix). These similarities may seem to imply that Li is simply replacing Mg on an atom-for-atom basis in the crystal lattice. More thorough examination of the data suggests this is not the case.

Figure 15 compares true stress at 0.1 true strain versus strain-rate for three alloy compositions: the 8 and 10wt.% Al-Mg binary alloys studied by Self [Ref. 15: pp. 48-49]; the 8 and 10wt.% Al-Mg Zirconium-containing alloys studied by Alcamo [Ref. 17: pp. 46-47, 62]; and the Li containing alloys investigated by this author. All test specimens were warm rolled and then isothermally deformed at 300°C; however, the degree of warm working among the three was unequal. The specimens tested by Self and Alcamo were warm rolled to a 94% reduction, while the Li containing alloys received only an 85% reduction. The data of both Self and Alcamo show a decrease in flow stress, and an increase in the strain-rate sensitivity coefficient, m, with increasing Mg concentration. The reason for the slight increase in flow stress of the Al-8%Mg-0.1%Zr above that of the Al-8%Mg binary is unclear.

Comparison of the 8 and 10wt.% Mg, Zr-containing alloys [Ref. 17: pp. 46-47, 62], with the Li-containing alloys of this research reveals that increased Li concentrations produce an effect similar to that produced by increases in weight percent Mg alone: decreased flow stress and larger m (Fig. 16). The composition of the Li alloys in atomic percent is Al-8.7%Mg-1.9%Li-0.05%Zr and Al-8.6%Mg-3.7%Li-0.05%Zr. If we pursue

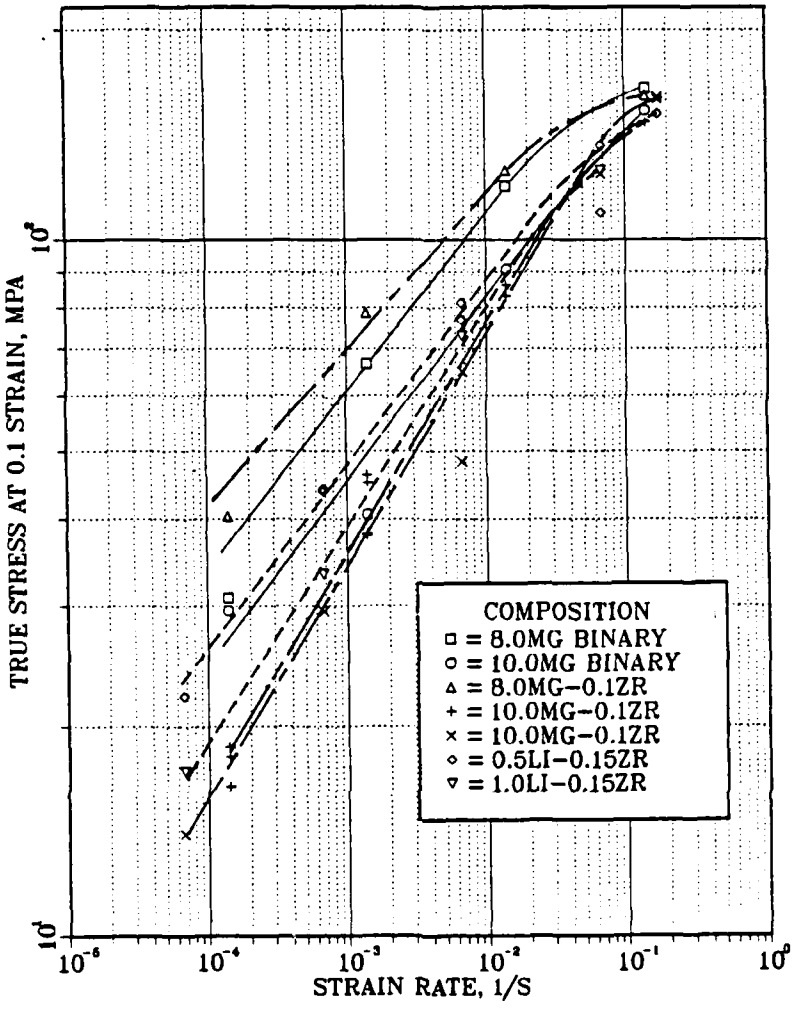

Figure 15. True Stress at 0.1 True Strain Plotted Against Strain Rate. Six compositions are represented. Increasing Mg content lowers flow stress and increases strain rate sensitivity coefficient, m. Increased Li additions produce similar result.

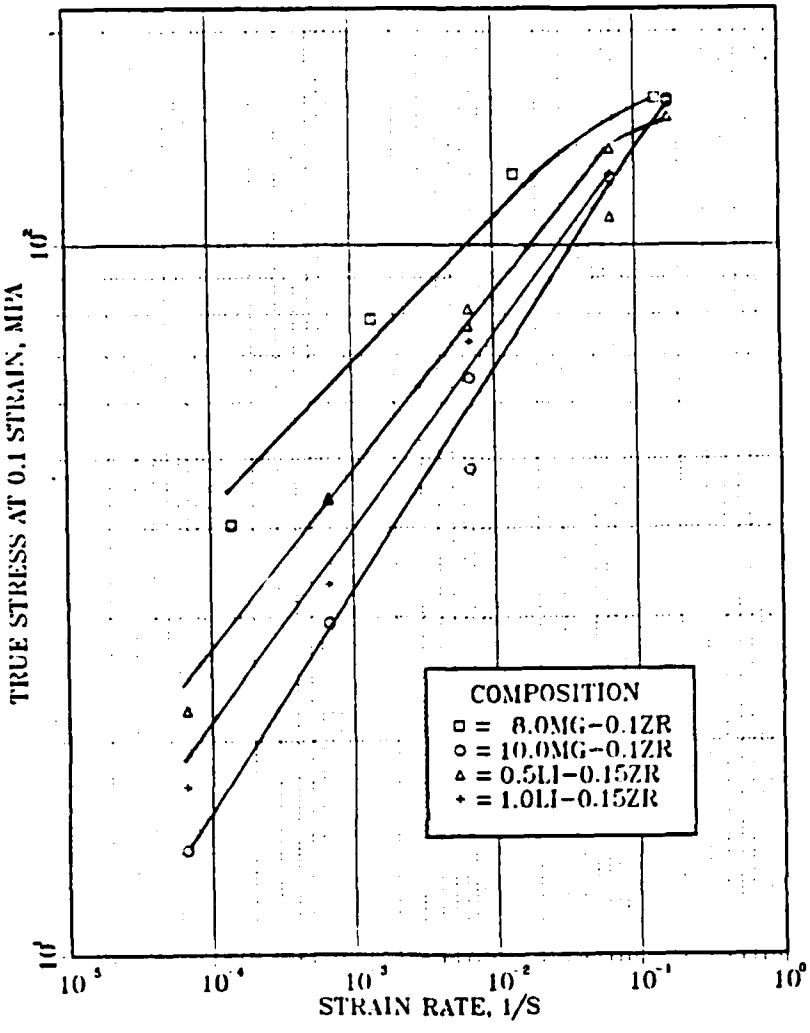

Figure 16. True Stress at 0.1 True Strain Plotted Against Strain Rate. Two compositions are presented to demonstrate the reduction in flow stress, and increase in m with an increase in either Mg or Li concentration.

the suggestion that Li replaces Mg on an atom-for-atom basis in the lattice, we would expect to see mechanical behavior consistent with "equivalent" Al-Mg-Zr alloys of composition 10.6 at.% Mg and 12.3 at.% Mg respectively. That is, if the suggestion were correct, one might reasonably expect to see a reduction in flow stress below that reported by Alcamo for 11 at.% Mg. This is not the case, however, as may be seen in both Figures 15 and 16. It is conceded that the differences in the original rolling reduction during TMP introduce additional uncertainty as to the cause of the observed differences. Larger reductions would produce a finer initial grain size in the Li alloys resulting in a lower flow stress, and a larger value of m. Alternative explanations appear more likely. McNelley and Garg [Ref. 18: pp. 917-920], for instance, have shown that thermomechanical processing at temperatures just below the solvus for Mg in Al-10.2%Mg reduced the Mg in solution to roughly the solubility limit of Mg in Al at the processing temperature. It is not unreasonable, therefore, to expect that increasing Mg content will produce a corresponding increase in the volume fraction of second phase ß precipitated. Self [Ref. 15: p. 55] and Alcamo [Ref. 17: p. 50] both suggested that increased precipitation of intermetallic ß exerted a refining effect on grain size in the alloys studied. Comparison of the three alloy compositions in Figures 15 and 16 supports their observation and suggests that, all other

variables being equal, the volume fraction of precipitated ß, Mg_5Al_8, is the most influential factor affecting flow stress and strain-rate sensitivity. How Li additions effect volume fraction ß is explored in section 4 below.

2. Li as a Strengthening Addition

As reported in chapter IV, both ambient and warm temperature strengths declined with increasing Li concentration. Comparison of Table II with the Table IV and V data obtained by Self [Ref 15: pp. 51-52] reveals that Li is not as effective as Cu, or Cu and Mn in combination for improving room temperature strengths.

B. OBSERVATION OF CONTINUOUS RECRYSTALLIZATION

1. Grain Coarsening

The family of curves in Figure 14 represent a plot of true stress at various fixed strains as a function of strain rate during elevated temperature tensile testing. The increase of flow stress with increase in strain indicates that strain hardening is occurring. Recalling the exponential dependence of stress on grain size during SPD, one might infer that microstructural coarsening (i.e., grain growth) is occurring in these alloys. This is in fact the case.

TEM examination of superplastically deformed specimens revealed that microstructural coarsening did occur, and that such coarsening was by continuous recrystallization rather than conventional nucleation and growth of new strain-free grains (Figs. 8, 9). The TEM micrograph of Figure 8 shows this continuous recrystallization as typically occurring in both Li containing alloys. Presence of the large, irregular precipitates (c), identified as β, on grain boundaries and at triple points suggests that they may act to control grain size by pinning of the grain boundaries. Interaction of a migrating subgrain boundary with the large, approximately spheroidal precipitate at (a) suggests that it too may exert a retarding influence on the rate of coarsening. The relative absence of individual dislocations in grain and subgrain interiors is also a noteworthy feature. This suggests that predominantly diffusional mechanisms such as grain boundary sliding are responsible for the superplastic response of these alloys, rather than dislocation generation and recovery mechanisms.

2. Identification of Precipitates

The ternary phase diagram for Al-Mg-Li, and the apexes of the ternary fields appear in Figure 17, and Table VI respectively [Ref. 4: p. 555]. Values in Table VI for 300°C were obtained by interpolation. Entering Table VI for 300°C indicates the potential presence of three equilibrium

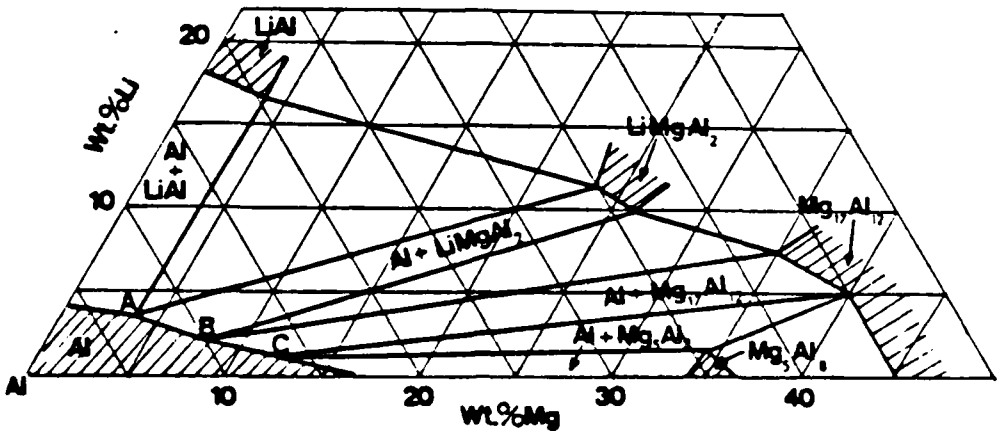

Figure 17. Aluminum Corner of the Al-Mg-Li System, T=467°C.

TABLE VI. APEXES OF AL-LI-MG TERNARY PHASE FIELDS, T=467°C.

	427°C		300°C		202°C	
	%Li	%Mg	%Li	%Mg	%Li	%Mg
(A) Al + LiAl + $LiMgAl_2$	2.2	3.0	1.5	2.4	1.0	2.0
(B) Al + $LiMgAl_2$ + $Mg_{17}Al_{12}$	1.2	7.0	0.7	5.0	0.3	3.4
(C) Al + $Mg_{17}Al_{12}$ + Mg_5Al_8	0.5	12.5	0.3	7.5	0.2	3.6

precipitates during elevated temperature deformation: $LiMgAl_2$, $Mg_{17}Al_{12}$, and Mg_5Al_8 . The large irregular precipitates so prevalent on grain boundaries were earlier identified as ß. SADP also identified the fine dispersoids as the metastable δ' phase, $LiAl_3$ [Ref. 23]. The warm working temperature is above the solvus for this phase, it therefore forms on cooling and is not present during SPD.

3. Connection Between Volume Fraction ß, Flow Stress, and m

A pattern of behavior has begun to emerge from the data presented thus far. The following important observations bear repeating:

- The $1/d^b$ dependence of strain-rate on grain size is well established for SPD, as dicussed in chapter II.

- The requirement for uniformly fine grain size may be seen from equation 2.3 where, if strain rate is to remain constant while grain size d increases, then stress must necessarily increase during deformation.

- Microstructural analysis using TEM suggests that pinning of grain boundaries by the ß phase is the most significant mechanism inhibiting grain growth.

- McNelley and Garg [Ref. 18: pp. 917-920] reported the ß phase to have precipitated during warm rolling of Al-10.2% Mg.

- The data of Self [Ref. 15] and Alcamo [Ref. 17] was examined. In both studies, increasing Mg content produced an increase in the value of m, and a decrease in flow stress during SPD.

- Increasing Li content in the present Al-Mg-Li-Zr alloys prompted a similar response.

It is infered from these facts that the volume fraction of precipitated ß is the most significant factor affecting recrystallized grain size in these alloys. As grains are continuously recrystallized from the deformed matrix, their high-angle boundaries are pinned by the ß phase particles. By increasing the volume fraction of ß, the inter-particle spacing of the ß phase is necessarily reduced (assuming the particles remain of similar size). A reduction of inter-particle spacing leads in turn to a finer initial grain size which, by the empirical relationships describing SPD, ought to reduce flow stress and raise the value of m. Such a model appears consistent with the behavior observed in the previously examined Al-Mg-X alloys.

a. The Additional Influence of Li

The interaction of migrating subgrain boundaries with large, approximately shperoidal precipitates (Fig. 8) suggests that that these precipitates may serve to retard the rate of grain coarsening in the Li-containing alloys. Such a restriction of coarsening may well be responsible for the reduction in flow stress seen for the Li-containing alloys despite their lesser degree of warm working. The identity of these

precipitates has not been established, but their presence is not reported in the earlier work at NPS. This suggests that the precipitate is eitner the Li-containing phase $LiMgAl_2$, or $Mg_{17}Al_{12}$ neither of which are expected in Al-Mg or Al-Mg-Zr alloys. Table VI indicates that the solubility of Li in Al-Mg remains relatively high at 300°C, on the order of 1.0wt.%. The possibility exists, therefore, that solute-drag may help to stabilize grain size either in conjunction with, or exclusive of the influence exerted by the unidentified precipitate.

b. Presence of Fine Dispersoids

Figures 8 and 9 both reveal the presence of fine, sub-micron dispersoid particles in grain interiors. Reference to Table VI and Figure 17 suggests it is unlikely that this phase is present at the temperature of SPD. Data for aging times of Al-Li-Mg alloys examined by Thompson [Ref. 5: pp. 111-115] suggest that the solvus for this phase is approximately 250°C. However, if these dispersoids are present during SPD, their scale is of the order necessary to introduce the possiblity of yet another grain refining mechanism namely the Zener-drag retardation of migrating boundaries. Interaction with such particles is capable of reducing boundary and subboundary mobility therby inhibiting the rate of grain growth.

4. Grain Growth

Comparison of Figures 8 and 9 clearly demonstrates the occurence of grain growth in these alloys. Both specimens received 85% reduction by warm rolling at 300°C, followed by SPD at the same temperature. The duration of SPD for the specimen in Figure 8 was 1 hour and 50 minutes, while that of the specimen in Figure 9 was 17 hours. The times required for pre-heating of specimens to 300°C were approximately equal, and were less than 60 minutes.

While no thoroughly sufficient explanation of continuous recrystallization yet exists, in observing the transition from the as-rolled microstructure seen in Figure 7 to the SPD microstructure of Figures 8 and 9, certain general observations in keeping with known recrystallization behavior may be made. The presence of the large, approximately spheroidal precipitates in the grain interior of Figure 9, the apparent pinning of grain boundaries by precipitated ß, and the near absence of subgrain boundaries suggest the following sequence of events for microstructural coarsening during elevated temperature testing of these alloys:

1. Continuous recovery by polygonization of dislocation tangles into cell walls forming low-angle or subgrain boundaries.

2. Migration and coalesence of subgrains to form high-angle grain boundaries.

3. Pinning of grain boundaries by ß precipitates.

4. Restricted grain growth.

It is important to note in connection with step 5 that both Berthold [Ref. 16: pp. 54, 81] and Alcamo [Ref. 17: pp. 72-73] report no discernable coarsening of the microstructure after initial recovery and continuous recrystallization had occurred in specimens undergoing isothermal annealling only. Appearance of the stable grain size was reported within the first 60 minutes of annealing. Grain growth did occur in specimens subjected to SPD, however. One may infer from such evidence that the growth mechanism in these thermomechanically processed alloys is diffusion controlled, but accelerated by deformation.

The model proposed by McQueen and Jonas may well play a role in the continuous recrystallization observed in both the Al-Mg-X and Al-Mg-Li-X alloys examined here. The schematic representation (Fig. 18) seems to explain their behavior quite well:

> (a) During cold deformation, a cellular substructure develops as the strain increases; by about 0.5 the cells reach their limiting size and thereafter the cell walls become much more dense. (b) Recovery during annealing commences with the annihilation of dislocations in the cell walls which turn into subboundaries. As recovery continues, the subgrains grow in diameter and the overall dislocation density decreases. (c) In hot working, subgrains develop in the strain hardening stage and reach an equilibrium size which is maintained during steady state flow. (d) In metals of high stacking fault energy, cells such as A, B, and C, coalesce

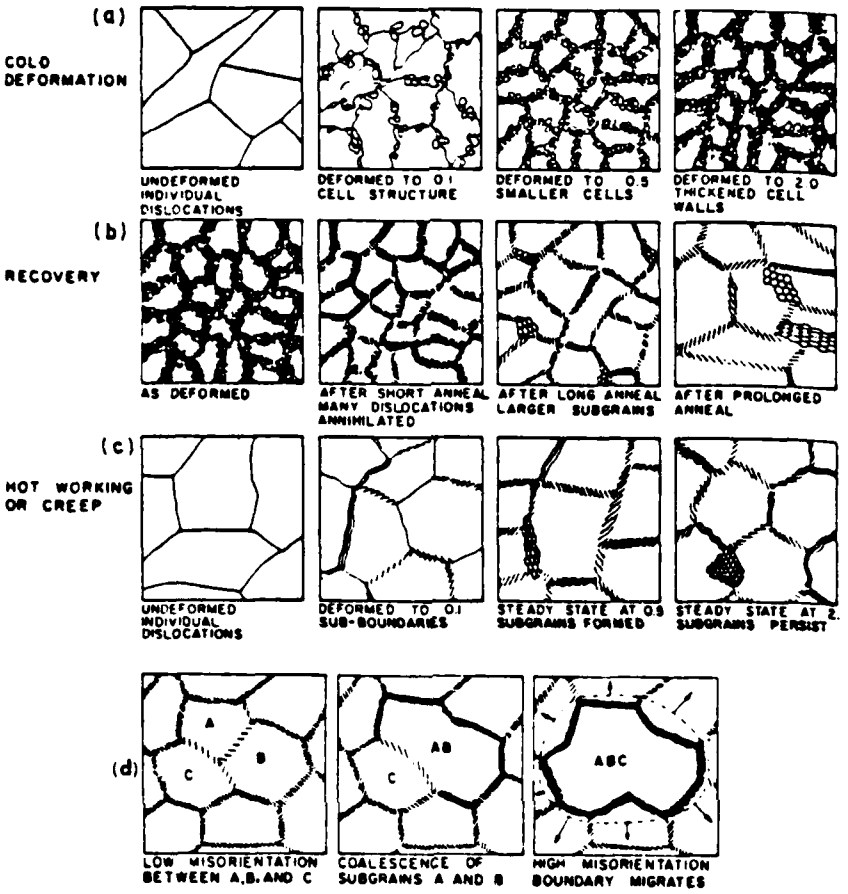

Figure 18. Schematic Representation of Discontinuous Recrystallization. Schematic due to McQueen and Jonas [Ref. 14].

into a crystallite to form a nucleus. This occurs as a result of the dislocations between the cells moving to surrounding subboundaries and increasing their misorientation until they can migrate freely. [Ref. 14: pp. 396-401]

A logical extension of this model to the present alloys requires only that, rather than further unrestricted growth, migration of the newly formed high-angle boundary is halted due to pinning by intermetallic ß precipitates.

5. The Apparent Value of m

Values for m typically approach 0.5 where extensive SPD has been reported. The values of the strain-rate sensitivity coefficient, m, for the 0.5wt.%Li and 1.0wt.%Li alloys are approximately 0.25 and 0.31 respectively. These values are relatively low, therefore, for metals exhibiting superplastic behavior, and one may be tempted to interpret these data as resulting from dislocation creep processes. However, microstructural data is inconsistent with such an interpretation in that, as reported earlier, recovery and recrystallization become more pronounced with increasing time and strain. That is, rather than development of dislocation sources and pile-ups there is a decrease in dislocation density with increasing time and strain. The low value of m observed in the present alloys is thought to result from a "masking" of of the true value due to grain growth. Application of equation 2.2 to true stress-strain rate will reveal a true

value of m only so long as grain size remains constant. Since the time required to achieve a fixed strain varies over the range of strain-rates tested, the length of time available for microstructural coarsening at lower strain-rates will be substantially greater. As coarsening occurs, the stress for a given strain would be expected to rise. This has the effect of decreasing the slope of the stress versus stran-rate curve, and hence the apparent value of m. It is highly probable, therefore, that the low values of m seen in these alloys are not accurate. Obtaining correct values will require experimental procedures such as described by Backofen [Ref. 7]. This method is more accurate, but is not used in the present work because the experimental procedure is more elaborate, and determining precise values for m was considered beyond the scope of this preliminary investigation.

VI. Conclusions.

The following conclusions are drawn from the data presented in the previous chapters:

1. Optical microscopy reveals that thermomechanical processing of both the 0.5%Li and 1.0%Li alloys produces an elongated grain structure with precipitation of intermetallic phases in a manner similar to Al-Mg-X alloys studied previously. The remarkably homogeneous microstructure makes it attractive for commerical use, especially if these marerials are moderately superplastic at warm temperatures.

2. Mechanical test data reveal strength-ductility combinations that are comparable to those of binary and ternary alloys previously studied at NPS.

3. Li is not as effective a strengthening addition as Cu, or Cu and Mn in combination. Increased alloying in previous high-magnesium Al-Mg alloys produced increases in strength. Increases in weight percent Li lead to reduced ambient and warm temperature strengths in these alloys.

4. Transmission electron microscopy reveals the presence of three distinct precipitate morphologies. The ternary phase diagram suggests the potential presence of three equilibrium precipitates during superplastic deformation at 300°C: $LiMgAl_2$, $Mg_{17}Al_{12}$, and Mg_5Al_8. SADP confirm the presence of ß (Mg_5Al_8).

5. Mechanical test data suggest microstructural coarsening during elevated temperature testing. TEM micrographs concur and reveal

that such coarsening occurs by continuous recrystallization rather than the nucleation and growth of new strain-free grains.

6. Comparison with previously studied binary and ternary Al-Mg alloys suggests that, for a fixed temperature, the volume fraction of ß precipitated is the most influential factor affecting flow stress, and strain-rate sensitivity coefficient, m.

7. The Al-Mg-Li alloys tested are moderately superplastic. It is suspected that greater initial reductions during warm rolling would confer higher ductilities.

VII. SUGGESTIONS FOR FUTURE RESEARCH

Based on the results of this thesis, Al-Mg-Li-Zr alloys appear to show promise as moderately superplastic materials of low density, good ductility and strength, with potential for improvement through control of the microstructural development by TMP. It is therefore suggested that the following studies be conducted:

1. A complete characterization of microstructural evolution during SPD to include:

   - Static annealling of as-rolled Al-Mg-Li-Zr specimens presently on-hand, followed by examination with TEM to determine the initial stable grain size prior to SPD.

   - Examination by TEM of the existing SPD specimens deformed at higher strain rates ($>10^{-4}$) to determine the rate of microstructural coarsening.

   - Warm rolling of these alloys to 94% reduction to help confirm the role that degree of prior working has in the superplastic behavior of these alloys.

   - Reproduce the experiments conducted in this study at higher Mg concentrations to determine percent elongation achieved by Al-10%Mg-0.5%Li-0.15%Zr and Al-10%Mg-1.0%Li-0.15%Zr alloys during SPD. This will help to confirm the role that volume fraction ß plays in stablizing the grain size.

- Collect data on the Al-8%Mg-1.5%Li-0.15%Zr and Al-8%Mg-2.0%Li-0.15%Zr to determine effect of Li additions at higher concentrations. If the role of Li-containing second phases is significant in restricting the rate of microstructural coarsening, then one may expect to see a finer recrystallized grain size, increases in both elongation and the apparent value of m, and a decrease in flow stress.

- Investigate the effects of temperature and strain rate for a temperature range comparable to that covered by Hartmann (20°C - 450°C) [Ref. 24].

2. Employ the differential scanning calorimeter (DSC) to aid in determining the times and temperatures at which recrystallization occurs in these alloys.

APPENDIX

TABLE II. MECHANICAL TEST DATA FOR AL-8%MG-0.5%LI-0.15ZR

Temp (C)	Strain Rate (sec^{-1})	YS Ksi (MPa)	UTS Ksi (MPa)	Ductility (Percent Elong.)
20	8.3×10^{-4}	32.1 (221.3)	64.73 (446.3)	10.3
		40.1 (276.5)	63.56 (438.2)	12.0
		42.0 (289.6)	63.76 (439.6)	12.0
		43.6 (300.6)	65.34 (450.5)	11.0

Temp (C)	Strain Rate (sec^{-1})	UTS Ksi (MPa)	True Stress at 0.1 True Strain Ksi (MPa)	Ductility (Percent Elong.)
300	1.7×10^{-1}	21.29 (146.8)	22.00 (151.7)	128.
	6.7×10^{-2}	17.96 (123.8)	19.81 (136.6)	133.
		16.10 (111.0)	15.90 (109.6)	174.
	6.7×10^{-3}	10.13 (69.84)	11.15 (76.88)	230.
		10.80 (74.46)	11.79 (81.29)	216.
	6.7×10^{-4}	5.93 (40.89)	6.35 (43.78)	274.
		5.79 (39.92)	6.40 (44.13)	293.
	6.7×10^{-5}	3.13 (21.58)	3.21 (22.13)	252.

TABLE III. MECHANICAL TEST DATA FOR AL-8%MG-1.0%LI-0.15%ZR

Temp (C)	Strain Rate (sec^{-1})	YS Ksi (MPa)	UTS Ksi (MPa)	Ductility (Percent Elong.)
20	8.3×10^{-4}	40.9 (282.0)	60.84 (419.5)	8.0
		38.3 (264.1)	60.38 (416.3)	10.6
		40.3 (277.9)	60.50 (417.1)	10.5

Temp (C)	Strain Rate (sec^{-1})	UTS Ksi (MPa)	True Stress at 0.1 True Strain Ksi (MPa)	Ductility (Percent Elong.)
300	6.7×10^{-2}	16.40 (113.1)	18.25 (125.8)	226.
	6.7×10^{-3}	9.50 (65.50)	10.58 (72.95)	216.
	6.7×10^{-4}	4.36 (30.06)	4.83 (33.30)	291.
	6.7×10^{-5}	2.44 (16.82)	2.50 (17.24)	343.

TABLE IV. MECHANICAL PROPERTIES OF AL-8%MG-0.4%CU [Ref. 15]

Temp (C)	Strain Rate (sec^{-1})	UTS (MPa)	True Stress at 0.1 True Strain (MPa)	Ductility (Percent Elong.)
20	5.3×10^{-5}	453.0	*	13.0
	5.3×10^{-4}	463.0	*	11.0
	5.3×10^{-3}	451.0	*	8.0
300	5.3×10^{-5}	22.0	*	210.0
	5.3×10^{-4}	30.0	*	224.0
	5.3×10^{-3}	63.0	79.2	152.0

* Specimen fractured before attaining 0.1 true strain.

TABLE V. MECHANICAL PROPERTIES OF AL-8%MG-0.4%CU-0.5%MN [Ref. 15]

Temp (C)	Strain Rate (sec^{-1})	UTS (MPa)	True Stress at 0.1 True Strain (MPa)	Ductility (Percent Elong.)
20	1.39×10^{-3}	473.9	*	16.3
	1.39×10^{-2}	474.3	*	11.8
300	1.39×10^{-4}	24.1	23.4	213.7
	1.39×10^{-3}	44.1	48.0	315.8
	1.39×10^{-2}	86.1	94.4	155.0
	1.39×10^{-1}	151.2	157.5	77.5

* Specimen fractured before attaining 0.1 true strain.

LIST OF REFERENCES

1. Rosenhain, W., Haughton, J.L., Bingham, K.E., J. Inst. Met., v. 23, p. 261, 1920.

2. Padmanabhan, K.A., and Davies, G.J., Superplasticity, Materials Research and Engineering, Volume 2, p. 58, Springer-Verlag, 1980.

3. Dieter, G.E., Mechanical Metallurgy, p. 213, McGraw-Hill, 1976.

4. Mondolfo, L.F., Aluminum Alloys: Structure and Properties, p. 555, Butterfield, 1976.

5. Thompson, G.E., and Noble, B., "Precipitation Characteristics of Aluminum-Lithium Alloys Containing Magnesium", J. Inst. Met., v. 101, pp. 111-115, 1973.

6. Wadsworth, J., Pelton, A.R., Lewis, R.E., "Superplastic Al-Cu-Li-Mg-Zr Alloys", Met. Trans., v. 16A, pp. 2319-2332, December 1985.

7. Backofen, W.A., Turner, I.R., Avery, D.H., Trans. Am. Soc. Met., v. 57, p.980, 1964.

8. Ruano, O.A., and Sherby, O.D., "Low Stress Creep of Fine-Grained Materials at Intermediate Temperatures: Diffusional Creep or Grain Boundary Sliding?", Material Science and Engineering, v. 56, pp. 167-175, 1982.

9. Orowan, E., and Scott, J.W., J. Iron Steel, v. 54, p. 45, 1946.

10. Weertman, J., J. Appl. Physics, v. 26, p. 1213, 1955.

11. Weertman, J., J. Appl. Physics, v. 28, pp. 1185-1189, 1957.

12. Smallman, R.E., Modern Physical Metallurgy, 4th Ed., pp. 363-366, Butterworths, 1985.

13. Wert, J.A., "Thermomechanical Processing of Heat Treatable Aluminum Alloys for Grain Size Control", Microstructural Control in Aluminum Alloys, pp. 67-94, The Metallurgical Society, Inc., 1986.

14. McQueen, H.J., and Jonas, J.J., "Recovery and Recrystallization During High Temperature Deformation", Treatise on Material Science Technology, v. 6, pp. 393-493, Academic Press, 1975.

15. Self, R.J., The Effect of Alloy Additions on Superplasticity in Thermomechanically Processed High-Magnesium Aluminum-Magnesium Alloys, M.S. Thesis, Naval Postgraduate School, Monterey, California, December 1984.

16. Berthold, D.B., Effect of Temperature and Strain Rate on Microstructure of a Deformed, Superplastic Al-10%Mg-0.1%Zr Alloy, M.S. Thesis, Naval Postgraduate School, Monterey, California, June 1985.

17. Alcamo, M.E., Effect of Strain and Strain Rate on the Microstructure of a Superplastically Deformed Al-10%Mg-0.1%Zr Alloy, M.S. Thesis, Naval Postgraduate School, Monterey, California, June 1985.

18. McNelley, T.R. and Garg, A., "Development of Structure and Mechanical Properties in Al-10.2%Mg by Thermomechanical Processing", Scripta Met., v. 18, pp. 917-920, 1984.

19. Divetcha, D., NSWC White Oak, Maryland, private communication, November 1985.

20. Klankowski, K.A., Retained Ambient Temperature Properties of Superplastically Deformed Al-10%Mg-0.1%Zr, Al-10%Mg-0.5%Mn, Al-10%Mg-0.4%Cu Alloys, M.S. Thesis, Naval Postgraduate School, Monterey, California, December 1985.

21. Metals Handbook, 9th ed., v. 9, pp. 351-360, American Society for Metals, 1985.

22. Anamet Laboratories Inc., Berkley, California, private communication, February 1986.

23. Hales, S.J., unpublished research, Naval Postgraduate School, Monterey, California, May 1986.

24. Hartmann, T.S., Mechanical Characteristics of a Superplastic Aluminum-10.2%Mg-0.1%Zr Alloy, M.S. Thesis, Naval Postgraduate School, Monterey, California, June 1985.

INITIAL DISTRIBUTION LIST

	No. Copies
1. Defense Technical Infromation Center Cameron Station Alexandria, Virginia 22304-6145	2
2. Library, Code 0142 Naval Postgraduate School Monterey, California 93943-5000	2
3. Department Chairman, Code 69Mx Department of Mechanical Engineering Naval Postgraduate School Monterey, California 93943-5000	1
4. Professor T.R. McNelley, Code 69Mc Department of Mechanical Engineering Naval Postgraduate School Monterey, California 93943-5000	5
5. Dr. S.J. Hales, Code 69Ha Department of Mechanical Engineering Naval Postgraduate School Monterey, California 93943-5000	1
6. Naval Air Systems Command, Code AIR 320A Naval Air Systems Command Headquarters Washington, DC 20361	1
7. LCDR Stephen B. Oster 6701 Kiowa Avenue, N.E. Albuquerque, New Mexico 87110	8

8. Dr. Jeffrey Waldman, Code 606 1
Naval Air Development Center
Warminster, Pennsylvania 18974

9. Dr. Eui-Whee Lee, Code 6063 1
Naval Air Development Center
Warminster, Pennsylvania 18974

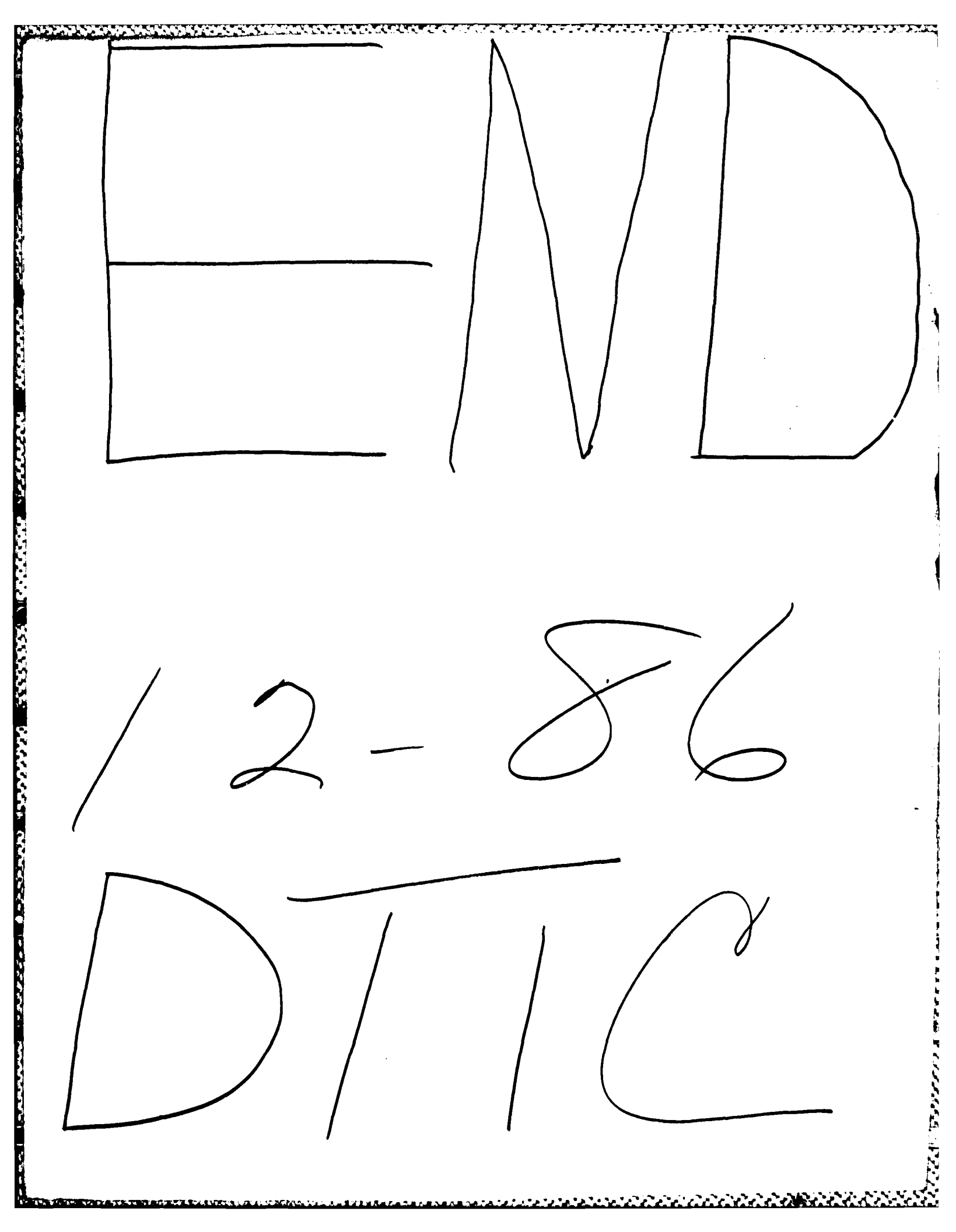
END
12-86
DTIC